cmgh
CELLULAR AND MOLECULAR GASTROENTEROLOGY AND HEPATOLOGY

ORIGINAL RESEARCH

SIRT6 Protects Against Liver Fibrosis by Deacetylation and Suppression of SMAD3 in Hepatic Stellate Cells

Xiaolin Zhong,[1,2,*] Menghao Huang,[2,3,*] Hyeong-Geug Kim,[2] Yang Zhang,[2] Kushan Chowdhury,[2] Wenjie Cai,[2] Romil Saxena,[4] Robert F. Schwabe,[5] Suthat Liangpunsakul,[2,3,6,7] and X. Charlie Dong[2,7]

[1]*Department of Gastroenterology, The Affiliated Hospital of Southwest Medical University, Luzhou, Sichuan Province, China;* [2]*Department of Biochemistry and Molecular Biology,* [3]*Division of Gastroenterology and Hepatology, Department of Medicine,* [4]*Department of Pathology and Laboratory Medicine,* [7]*Center for Diabetes and Metabolic Diseases, Indiana University School of Medicine, Indianapolis, Indiana;* [5]*Institute of Human Nutrition, Department of Medicine, College of Physicians and Surgeons, Columbia University, New York, New York;* [6]*Roudebush Veterans Administration Medical Center, Indianapolis, Indiana*

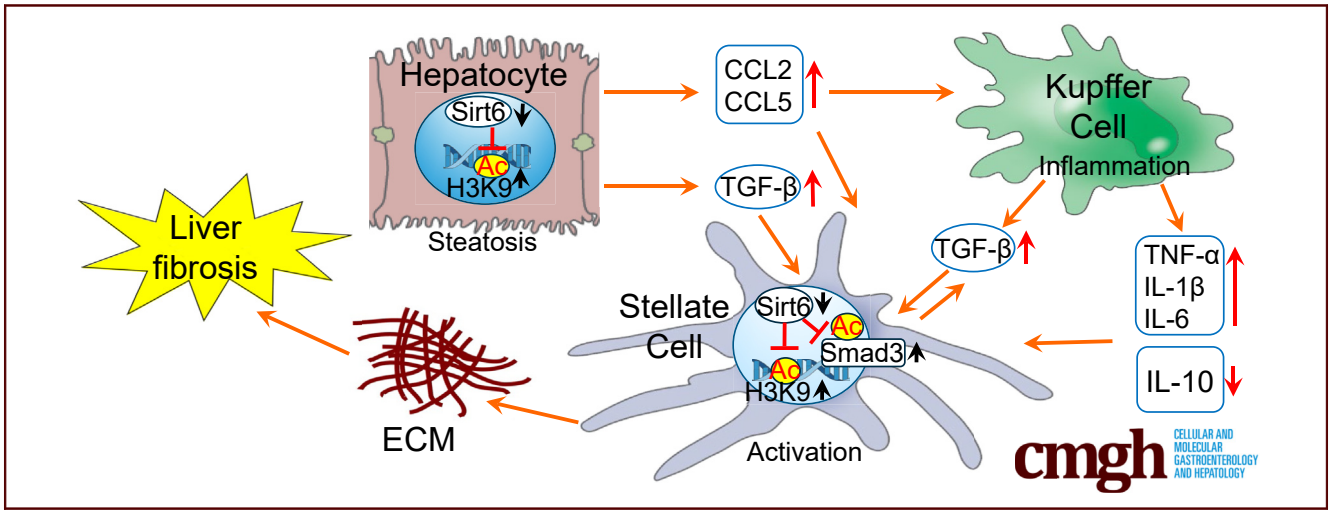

SUMMARY

This work characterized a key function of Sirtuin 6 (SIRT6) in the regulation of liver fibrosis. Mechanistically, SIRT6 deacetylates and suppresses SMAD family member 3 in hepatic stellate cells. Gain- and loss-of-function data show that SIRT6 is a potential therapeutic target for hepatic fibrosis.

BACKGROUND & AIMS: Nonalcoholic steatohepatitis (NASH) is a chronic liver disease that is manifested clinically by an increase in hepatic triglycerides, inflammation, and fibrosis. The pathogenesis of NASH remains incompletely understood. Sirtuin 6 (Sirt6), a nicotinamide adenine dinucleotide–dependent deacetylase, has been implicated in fatty liver disease; however, the underlying molecular mechanisms in the NASH pathogenesis are elusive. The aims of this study were to elucidate the role of hepatic Sirt6 in NASH.

METHODS: Wild-type, liver-specific *Sirt6* knockout (KO), hepatic stellate cell (HSC)-specific Sirt6 knockout (HSC-KO), and *Sirt6* transgenic mice were subjected to a Western diet for 4 weeks. Hepatic phenotypes were characterized and underlying mechanisms were investigated.

RESULTS: Remarkably, both the liver-KO and HSC-KO mice developed much worse NASH than the wild-type mice, whereas the transgenic mice were protected from the diet-induced NASH. Our cell signaling analysis showed that Sirt6 negatively regulates the transforming growth factor β–Smad family member 3 (Smad3) pathway. Biochemical analysis showed a physical interaction between Sirt6 and Smad3 in hepatic stellate cells. Moreover, our molecular data further showed that Sirt6 deacetylated Smad3 at key lysine residues K333 and K378, and attenuated its transcriptional activity induced by transforming growth factor β in hepatic stellate cells.

CONCLUSIONS: Our data suggest that SIRT6 plays a critical role in the protection against NASH development and it may serve as a potential therapeutic target for NASH. *(Cell Mol Gastroenterol Hepatol 2020;10:341–364; https://doi.org/10.1016/j.jcmgh.2020.04.005)*

Keywords: Sirtuin 6; Steatosis; Inflammation; Nonalcoholic Steatohepatitis; Deacetylation.

Nonalcoholic fatty liver disease (NAFLD) is an epidemic chronic liver disease that begins with simple steatosis and gradually progresses to nonalcoholic steatohepatitis (NASH), cirrhosis, and even liver cancer.[1] One of the common risk factors for NAFLD is overweight or obesity. Excessive energy intake is stored as triglycerides not only in the adipose tissue, but also in the liver and other tissues. Hepatic lipid accumulation can cause liver injury and cellular function impairment by an increase in reactive oxygen species, endoplasmic reticulum stress, and other tissue damage responses.[2] Hepatic tissue injury also triggers immune responses including the recruitment of circulated and resident macrophages and neutrophils, which lead to inflammation in the liver. Under the inflammatory conditions, hepatic cells secrete various cytokines and chemokines including transforming growth factor β (TGFβ) and chemokine (C-C motif) ligands 2 and 5. TGFβ is a potent fibrogenic factor that can trigger the activation of quiescent hepatic stellate cells (HSCs).[3] On TGFβ binding to its receptors 1/2, the receptor kinase phosphorylates and activates SMAD2 and SMAD3 transcription factors. Either SMAD family member 2 (SMAD2) or SMAD3 can form heterodimers with SMAD4 and then translocate to the nucleus for activation of numerous target genes including fibrogenesis genes such as *ACTA2*, *COL1A1*, and *COL3A1*.[4] In addition to phosphorylation, SMAD3 also is regulated positively by lysine acetylation, especially at lysine 378.[5]

It is believed that interactions between environmental factors such as diet and epigenetics play an important role in the development of NAFLD.[1] As a key epigenetic regulator, sirtuin 6 (SIRT6) has been implicated in the control of glucose and lipid metabolism, anti-oxidative stress, and anti-inflammation.[6–16] SIRT6 is a nicotinamide adenine dinucleotide–dependent deacetylase/deacylase.[17–19] Sirt6 deficiency in mice leads to hepatic steatosis and inflammation.[14,20–22] In addition, *Sirt6* whole-body knockout mice develop fibrosis in the heart, liver, kidneys, and lungs.[21,23] It has been suggested that regulation of the TGFβ–SMAD2/3 pathway by SIRT6 plays a role in tissue fibrosis.[23–25] However, the function and mechanism of SIRT6 in hepatic stellate cells remains unclear. In this work, we set out to illustrate the pathophysiological function of Sirt6 in mouse and human HSCs.

Results

Hepatic SIRT6 Is Decreased in NASH Patients and Diet-Induced NASH Mice

To examine the role of SIRT6 in human NASH pathogenesis, we analyzed hepatic SIRT6 protein levels in controls and patients with NASH. Hepatic SIRT6 was decreased by 3-fold in those with NASH compared with controls (Figure 1*A*), suggesting that SIRT6 might be involved in human NASH pathogenesis. To further examine whether SIRT6 is decreased progressively during fibrogenesis, we stained SIRT6 in liver biopsy specimens from NASH patients with different stages of NASH progression from simple steatosis to different degrees of hepatic fibrosis and cirrhosis. Our data showed that as the disease advanced to fibrosis and cirrhosis, nuclear SIRT6 levels were reduced markedly (Figure 1*B*), suggesting a potential role of SIRT6 in liver fibrosis. We also determined SIRT6 transcript levels by real-time polymerase chain reaction (PCR) analysis and found a significant decrease in hepatic SIRT6 messenger RNA (mRNA) levels in NASH patients (Figure 1*C*).

To assess the status of Sirt6 in NASH development in animal models, we fed wild-type (WT) C57BL6/J mice either a control or Western diet (WD) for 4 and 8 weeks and analyzed hepatic Sirt6 and Smad3. Our data showed that a WD induced a significant increase in hepatic steatosis and fibrosis at 4 weeks, and more so at 8 weeks (Figure 2*A*). Hepatic Sirt6 was decreased significantly and Smad2 and Smad3 phosphorylation levels were increased in the WD-treated mice (Figure 2*B*). Moreover, hepatic Smad3 acetylation was increased in the livers of the WD-treated mice (Figure 2*C*). These data suggest that hepatic SIRT6 is downregulated during NASH development in both human beings and mice. Because HSCs are critical for hepatic fibrogenesis, we also examined Sirt6 gene expression during HSC activation using mouse primary HSCs. Within 5 days of culture, primary HSCs were activated, as shown by an induction of *Col1a1* and *Acta2* genes. During the same time course, Sirt6 was decreased at both mRNA and protein levels (Figure 3*A–D*). In addition, Sirt6 mRNA levels also were decreased in the TGFβ-treated primary HSCs (Figure 3*E*). Taken together, our data suggest that Sirt6 might be involved in HSC activation and liver fibrosis.

Hepatic Sirt6 Protects Against Diet-Induced NASH in Mice

To further investigate the role of Sirt6 in the development of NASH, we generated liver-specific *Sirt6* knockout mice (KO; Alb–Cre-mediated) and whole-body *Sirt6* transgenic (Tg) mice. As shown by Western blot analysis, Sirt6 was ablated specifically in the liver of KO mice and overexpressed in both the liver and heart in Tg mice (Figure 4*A*). To model NASH development, we fed WT, KO, and Tg mice with a WD for 4 weeks. Although body weight did not change significantly, liver weight and the liver-to–body weight ratio were increased remarkably in the KO mice, but completely normalized in the Tg mice (Figure 4*B–G*). Liver morphology showed a typical fatty liver phenotype in the

*Authors share co-first authorship.

Abbreviations used in this paper: **ALT, alanine aminotransferase; ChIP, chromatin immunoprecipitation; DMEM, Dulbecco's modified Eagle medium; GFP, green fluorescent protein; HA, hemagglutinin; HSC, hepatic stellate cell; KO, knockout; Lrat, lecithin retinol acyltransferase; mRNA, messenger RNA; NAFLD, nonalcoholic fatty liver disease; NASH, nonalcoholic steatohepatitis; PBS, phosphate-buffered saline; PCR, polymerase chain reaction; shRNA, short hairpin RNA; SIRT6, sirtuin 6; SMAD3, SMAD family member 3; Tg, transgenic; TGFB, transforming growth factor β; WD, Western diet; WT, wild-type.**

Most current article

2352-345X
https://doi.org/10.1016/j.jcmgh.2020.04.005

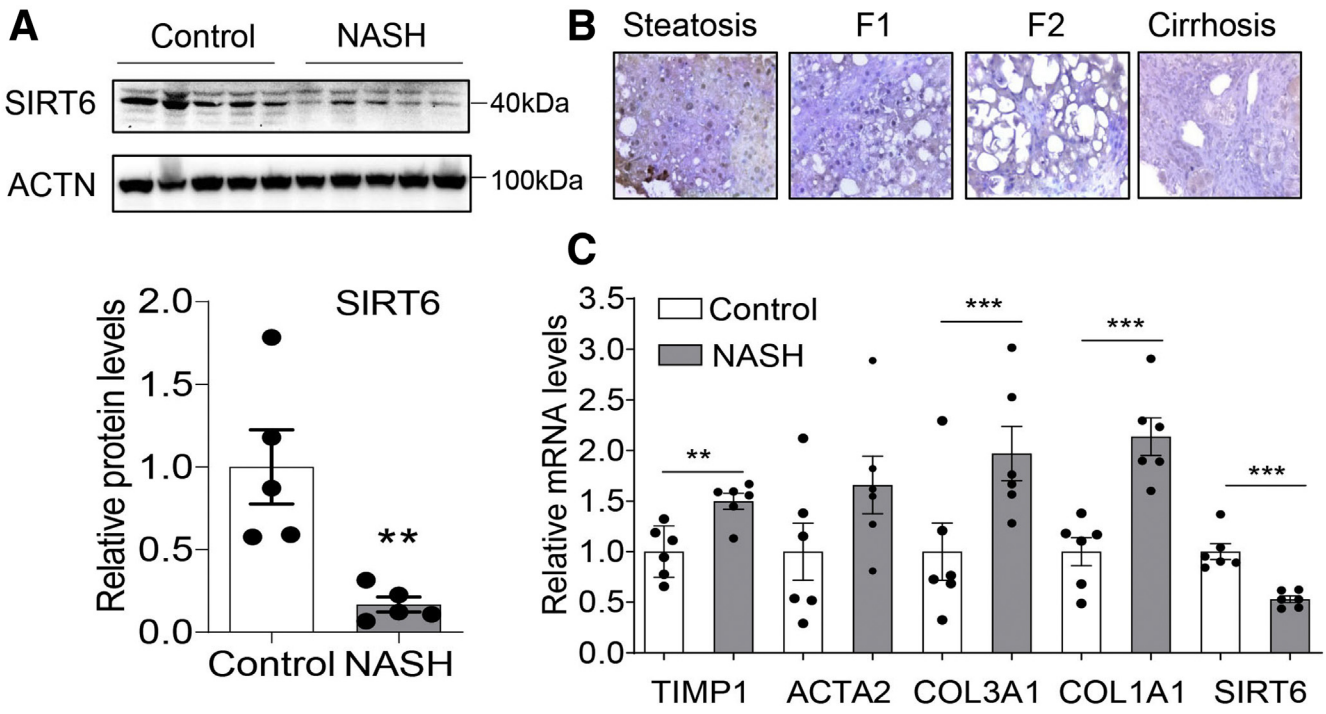

Figure 1. SIRT6 protein levels are decreased in the livers of NASH patients. (*A*) Western blot analysis and quantification of SIRT6 protein in the human liver samples from controls and NASH patients. (*B*) Immunohistochemical analysis of SIRT6 in human liver biopsy specimens from patients with simple hepatic steatosis, different grades of fibrosis, and cirrhosis. (*C*) Real-time PCR analysis of *TIMP1*, *ACTA2*, *COL3A1*, *COL1A1*, and SIRT6 in human liver samples from controls and NASH patients (n = 6). Data are presented as means ± SEM. $^{**}P < .01$ and $^{***}P < .001$. ACTN, actinin.

KO mice and no abnormal appearance in the Tg mice (Figure 4*H*). Biochemical analysis of hepatic triglycerides also showed a 2-fold increase in the KO mice and normalization in the Tg mice (Figure 4*I*). H&E staining and quantification of liver sections also confirmed that hepatic steatosis was much worse in the KO mice than in the WT mice, but normalized in the Tg mice (Figure 5*A* and *B*).

To assess hepatic inflammation, we performed immunohistochemistry for F4/80 (a macrophage marker) and myeloperoxidase (a neutrophil marker). Both markers were highly increased in the KO livers and nearly normal in the Tg mice (Figure 5*A* and *B*). Real-time PCR analysis showed that inflammatory cytokine genes including *Il1b* and *Tnf* were increased significantly in the KO livers and decreased dramatically in the Tg livers compared with the WT livers (Figure 5*C* and *D*). Serum alanine aminotransferase (ALT) levels were increased by 50% in the KO mice but nearly normal in the Tg mice compared with the WT mice (Figure 5*E*), indicating a protective role of Sirt6 against liver injury. In addition, liver injury–associated biliary ductular reaction was worsened in the KO mice compared with the WT mice (Figure 5*F*).

To examine hepatic fibrosis, we first performed Sirius Red staining of liver sections. Our data showed that KO mice developed much worse fibrosis than the WT mice, whereas the Tg mice were completely protected against fibrosis (Figure 6*A* and *B*). This fibrosis phenotype was corroborated by expression of fibrogenesis genes including *Col1a1*, *Acta2*, *Tgfb1*, and *Tgfbr1* (Figure 6*C*). To explore potential mechanisms, we analyzed Smad3 phosphorylation and acetylation, indicators of Smad3 activation. Our data showed that both modifications were increased in the KO, but decreased in the Tg, livers (Figure 6*D*). To examine whether there was any indication of epithelial–mesenchymal transition, we analyzed 2 common markers in the livers of WT and KO mice. Our data showed that E-cadherin was decreased by 75% and vimentin was increased by 4-fold in the KO livers (Figure 6*E*), suggesting that Sirt6 deficiency promotes epithelial–mesenchymal transition in the liver.

Sirt6 Deficiency Triggers Inflammation in Hepatocytes and Fibrogenesis in HSCs

A recent report showed that Alb-Cre is active in both hepatocytes and HSCs,[26] therefore we also analyzed *Sirt6* gene deletion in primary hepatocytes and HSCs in our Alb-Cre–mediated *Sirt6* KO mice. Indeed, Alb-Cre led to 70% *Sirt6* ablation in HSCs, whereas it mediated 90% *Sirt6* deletion in hepatocytes (Figure 7*A* and *B*). Immunofluorescent microscopy also confirmed the *Sirt6* deletion in HSCs and hepatocytes (Figure 7*C* and *D*). In addition, we also examined Sirt6 protein in cholangiocytes by staining liver sections. Our data showed that Sirt6 was depleted in only a small fraction of cholangiocytes in the KO mice (Figure 7*E*). Gene expression analysis in mouse primary hepatocytes and

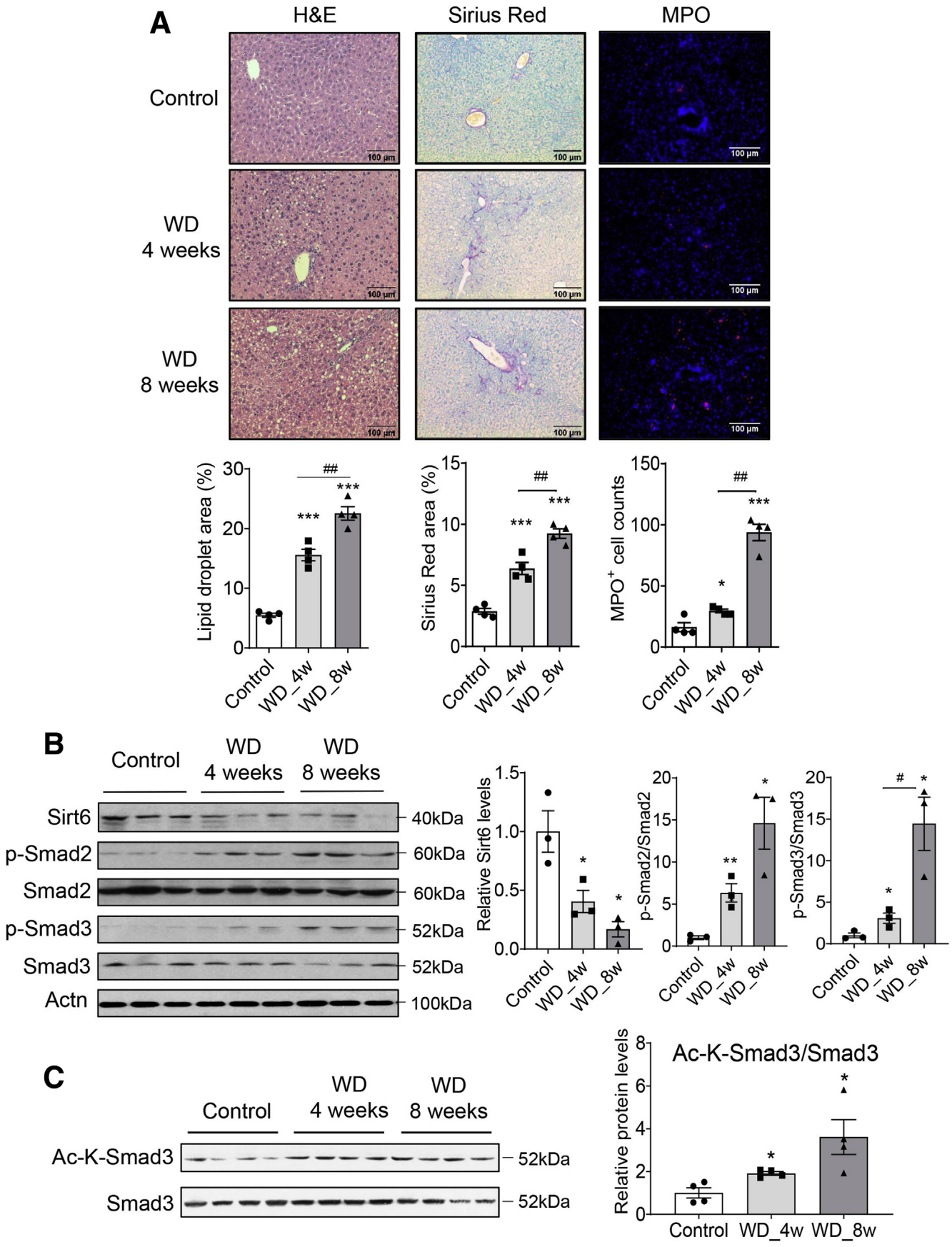
A
H&E
Sirius Red
MPO
Control
WD 4 weeks
WD 8 weeks
100 μm
Lipid droplet area (%)
Sirius Red area (%)
MPO+ cell counts
Control
WD_4w
WD_8w
B
Control
WD 4 weeks
WD 8 weeks
Sirt6
p-Smad2
Smad2
p-Smad3
Smad3
Actn
40kDa
60kDa
60kDa
52kDa
52kDa
100kDa
Relative Sirt6 levels
p-Smad2/Smad2
p-Smad3/Smad3
C
Ac-K-Smad3
Smad3
52kDa
52kDa
Ac-K-Smad3/Smad3
Relative protein levels

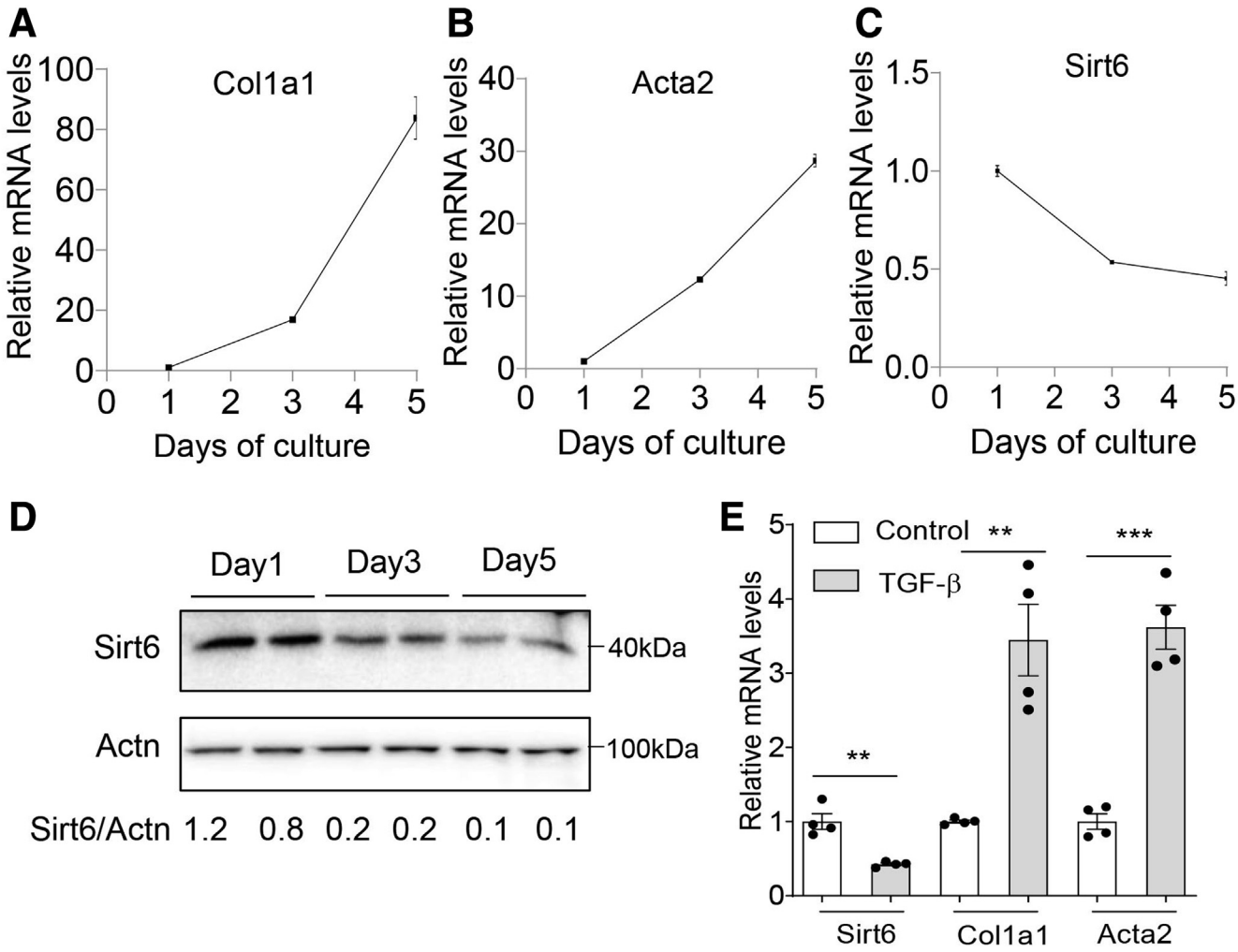

Figure 3. Sirt6 is down-regulated during HSC activation. (*A–C*) Real-time PCR analysis of *Col1a1*, *Acta2*, and *Sirt6* mRNAs in mouse primary HSCs after culture for 1–5 days (n = 3). (*D*) Western blot analysis of Sirt6 in mouse primary HSCs after culture for 1–5 days. (*E*) Real-time PCR analysis of Col1a1, Acta2, and Sirt6 mRNAs in mouse primary HSCs in the absence or presence of TGFβ1 (5 ng/mL) for 24 hours (n = 4). Data are presented as means ± SEM. $^{**}P < .01$ and $^{***}P < .001$ vs control. Actn, actinin; p-Smad, phospho-SMAD family member 2.

HSCs showed that a number of cytokine and chemokine genes including *Ccl2*, *Tgfb1*, *Ccl5*, and *Tnf* were highly increased in the hepatocytes whereas fibrogenesis genes such as *Col1a1*, *Col4a1*, *Timp1*, and *Tgfb1* were increased remarkably in the Sirt6-deficient HSCs compared with their WT counterparts (Figure 8*A* and *B*). We also performed co-culture experiments to test potential interactions between primary hepatocytes and HSCs. Although Sirt6-deficient HSCs did not further induce cytokine and chemokine gene expression in the KO hepatocytes, Sirt6-deficient hepatocytes enhanced fibrogenic gene expression in the KO HSCs (Figure 8*C* and *D*).

Sirt6 Deficiency in HSCs Increases the Susceptibility to Diet-Induced NASH in Mice

To investigate the in vivo function of Sirt6 in HSCs, we generated *Sirt6* HSC-KO mice by crossing the floxed *Sirt6* mice with a lecithin retinol acyltransferase (Lrat)-Cre line. Our data showed that *Sirt6* was deleted specifically in HSCs, but not hepatocytes or Kupffer cells (Figure 9*A–D*). Although there was no difference in body weight between WT and HSC-KO mice, both liver weight and liver-to–body weight ratio were increased significantly in the HSC-KO mice after 4 weeks of WD feeding (Figure 9*E–G*). HSC-KO mice had much worse hepatic inflammation, liver injury,

Figure 2. (***See previous page***). **Hepatic Sirt6 is down-regulated during NASH development in mice.** (*A*) H&E, Sirius Red staining, and immunofluorescence analysis of myeloperoxidase (MPO) and quantification of liver sections of control and WD-treated mice (4- to 6-month-old males, n = 4). (*D*) Western blot and quantification analysis of Sirt6, p-Smad2, Smad2, p-Smad3, and Smad3 in the livers of control and WD-treated mice. (*C*) Western blot and quantification of Smad3 acetylation (Ac-K-Smad3) in the livers of control and WD-treated mice. Data are presented as means ± SEM. $^{*}P < .05$, $^{**}P < .01$, and $^{***}P < .001$ vs control; $^{\#}P < .05$, and $^{\#\#}P < .01$ vs WD_4w.

and fibrosis than WT mice, as indicated by histologic markers, serum ALT, and HSC gene expression (Figure 10*A*–*E*). We also analyzed Smad3 phosphorylation in HSC-KO livers and HSCs and observed that phosphorylated Smad3 levels were increased remarkably (Figure 10*F*). Fluorescent microscopy also confirmed an increase in Smad3 phosphorylation and nuclear translocation in HSC-KO mouse primary HSCs (Figure 10*G*).

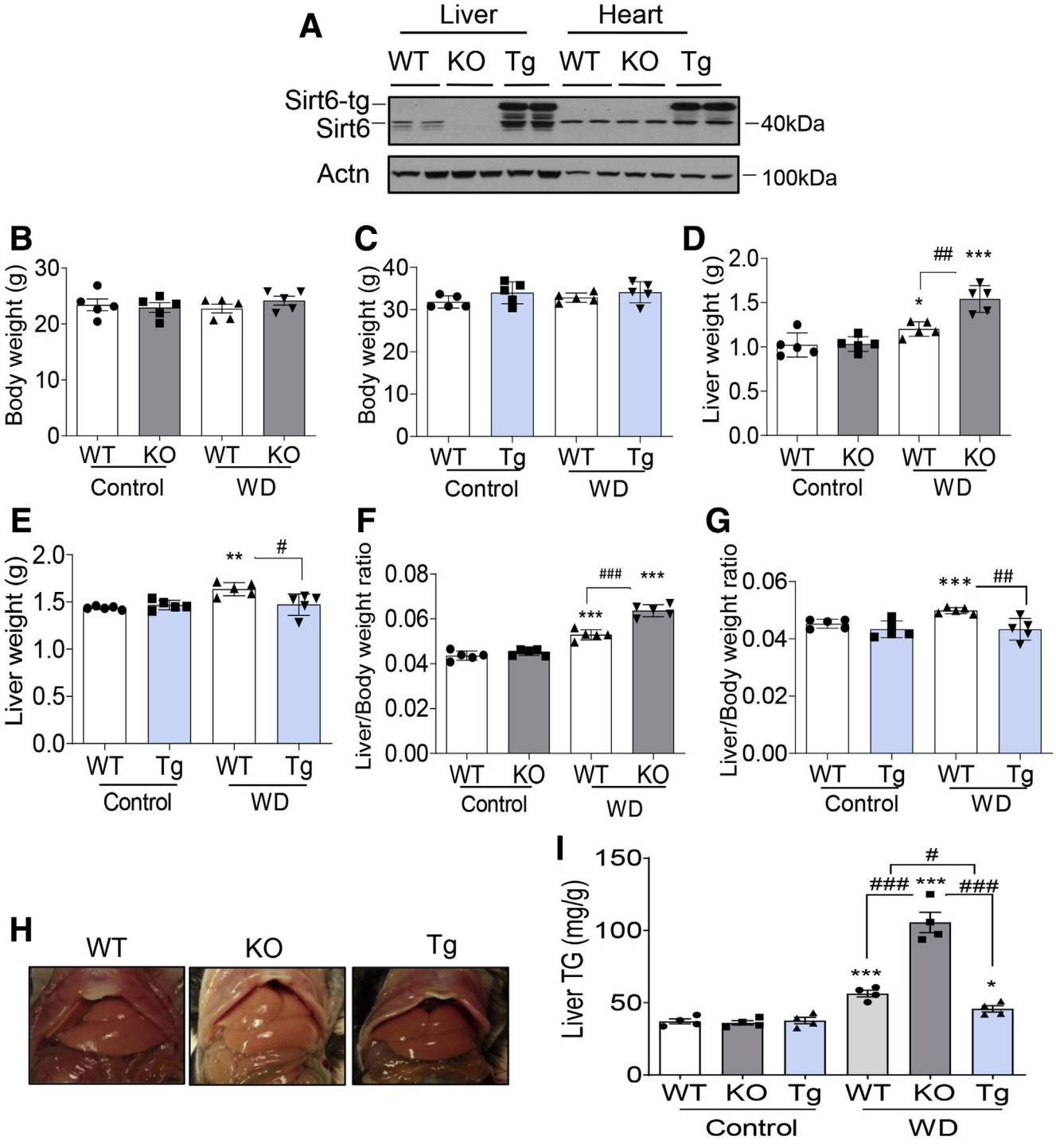

Figure 4. Sirt6 protects the liver from diet-induced hepatic steatosis. (*A*) Western blot analysis of Sirt6 protein in WT, Sirt6-KO, and Sirt6-Tg mouse liver and heart tissues. (*B* and *C*) Body weight measurements for Sirt6-KO vs WT and Sirt6-Tg vs WT mice (n = 5, 4- to 6-month-old males). (*D* and *E*) Liver weight measurements (n = 5). (*F* and *G*) Liver-to-body weight ratios (n = 5). (*H*) Gross images of livers of WT, Sirt6-KO, and Sirt6-Tg mice fed with WD for 4 weeks (4- to 6-month-old males). (*I*) Hepatic triglyceride (TG) measurements (n = 4). Data are presented as means ± SEM. $^{*}P < .05$, $^{**}P < .01$, and $^{***}P < .001$ for WD vs control for the same genotype; $^{\#}P < .05$, $^{\#\#}P < .01$, and $^{\#\#\#}P < .001$. Actn, actinin.

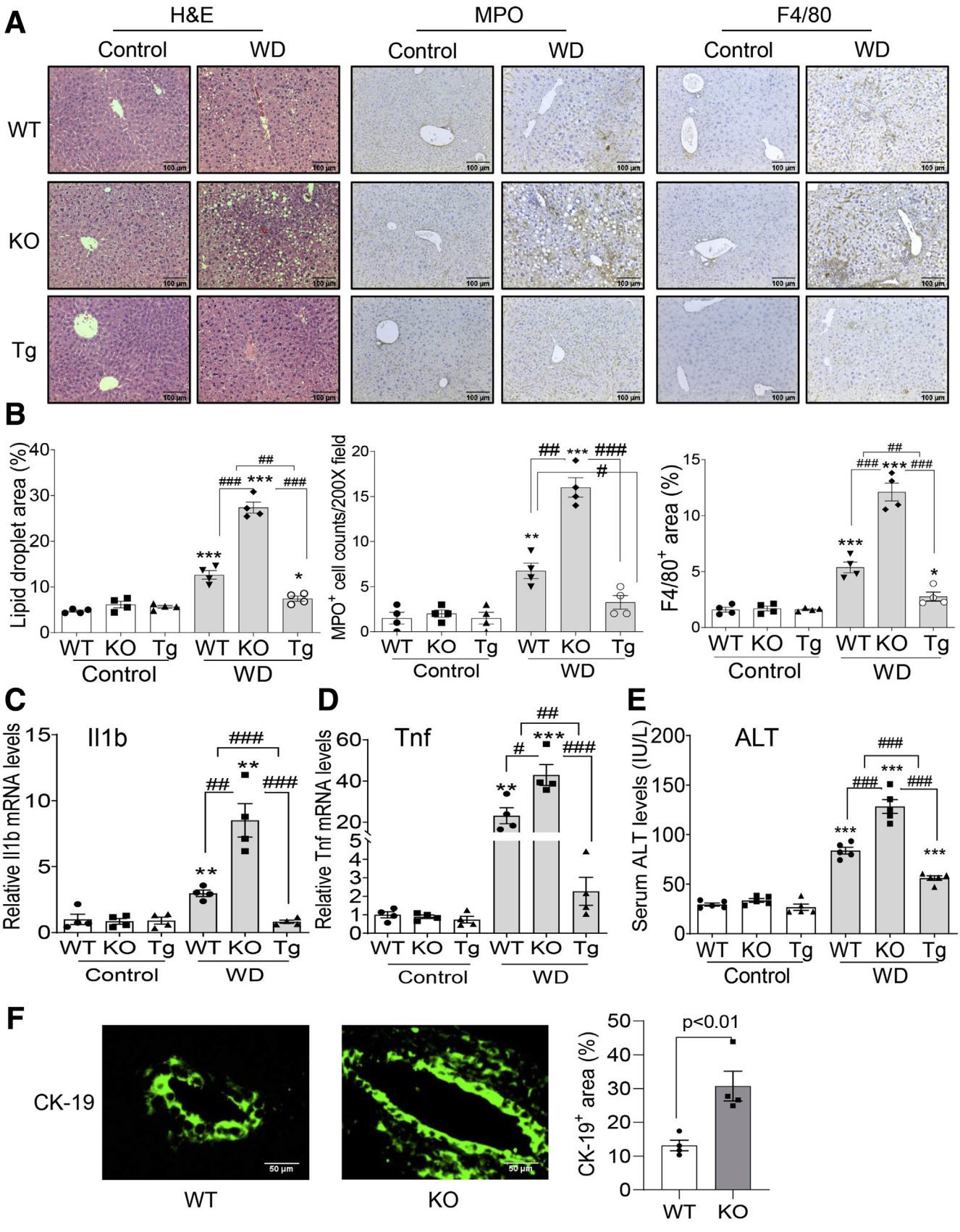
A
H&E
MPO
F4/80
Control
WD
WT
KO
Tg
100 μm
B
Lipid droplet area (%)
MPO+ cell counts/200X field
F4/80+ area (%)
WT KO Tg WT KO Tg
Control
WD
C
Il1b
Relative Il1b mRNA levels
D
Tnf
Relative Tnf mRNA levels
E
ALT
Serum ALT levels (IU/L)
F
CK-19
50 μm
WT
KO
CK-19+ area (%)
p<0.01

Sirt6 Represses the TGFβ-SMAD3 Pathway in HSCs

To further examine the role of SIRT6 in HSCs, we selected the human HSC cell line LX-2, which is used commonly for hepatic fibrosis study. First, we knocked down the *SIRT6* gene in the LX-2 cells using short hairpin RNAs (shRNAs) and cultured the cells in the absence or presence of TGFβ. Knockdown of *SIRT6* significantly enhanced TGFβ-stimulated SMAD3 phosphorylation (Figure 11*A*). Second, we performed SIRT6 overexpression in the LX-2 cells. Western blot data showed that overexpression of SIRT6 significantly decreased the TGFβ-stimulated SMAD3 phosphorylation (Figure 11*B*). Third, we overexpressed catalytically inactive SIRT6 mutant (H133Y) in the LX-2 cells. Our data showed that the TGFβ-stimulated SMAD3 phosphorylation was not decreased by the mutant SIRT6 (Figure 11*E*), suggesting that the Sirt6 catalytic activity is required for the regulation of SMAD3 phosphorylation. Expression of fibrogenic genes including *COL1A1*, *COL3A1*, *ACTA2*, and *TIMP1* in the LX-2 cells also was consistent with the negative regulation of SMAD3 by SIRT6. Wild-type but not mutant SIRT6 overexpression repressed those fibrogenesis genes whereas SIRT6 knockdown enhanced their expression (Figure 11*C*, *D*, and *F*).

To further understand the molecular regulation of SMAD3 by SIRT6, we performed co-immunoprecipitation using either SIRT6 or phosphorylated SMAD3 antibodies. Our data showed that SIRT6 indeed interacted with both SMAD3 and its phosphorylated form (Figure 12*A* and *B*). We also performed affinity purification of Sirt6 protein complexes in liver lysates by taking advantage of the HA-tagged Sirt6 transgene in our Tg mice. Indeed, Sirt6-hemagglutinin (HA) co-purified with Smad3 and Foxo1 (a positive control) (Figure 12*C*). Fluorescent microscopy also showed nuclear co-localization of SIRT6 and SMAD3, especially after TGFβ stimulation (Figure 12*D* and *E*).

To analyze the effect of SIRT6 on SMAD3 acetylation, we knocked down or overexpressed wild-type or mutant SIRT6 (H133Y) and immunoprecipitated SMAD3 for acetylation analysis. Our data showed that *SIRT6* knockdown increased SMAD3 acetylation whereas overexpression of WT but not mutant SIRT6 decreased SMAD3 acetylation (Figure 13*A* and *B*), suggesting that SIRT6 catalytic activity is required for SMAD3 deacetylation. To verify the interaction between SIRT6 and SMAD3 in the chromatin context, we performed chromatin immunoprecipitation (ChIP)–PCR analysis of 2 known SMAD3 target genes: *TGFB1* and *COL1A2* in LX-2 cells. Our data showed that SIRT6 and acetylated histone H3 lysine 9 (a substrate of SIRT6) both were enriched in the SMAD3 binding sites in the *TGFB1* and *COL1A2* gene promoters (Figure 13*C*). To further characterize which lysine acetylation in SMAD3 is regulated by SIRT6, we mutated 2 previously reported lysine residues, K333 and K378, to arginine that cannot be acetylated. Our data showed that both mutations reduced the SMAD3 acetylation levels and K378 seemed to be a major deacetylation site by SIRT6 (Figure 13*D*). Real-time PCR analysis further confirmed that acetylation of both K333 and K378 was involved in the SMAD3 transcriptional activity and deacetylation by SIRT6 markedly attenuated the SMAD3 transcriptional activity (Figure 13*E*).

Discussion

SIRT6 has been implicated in multiple biological processes including glucose and lipid metabolism, inflammation, anti-oxidative stress, DNA repair, and tumor suppression.[6–17,20,22,27–44] In this work, we reported that SIRT6 is also a key regulator for liver fibrosis. Because NAFLD is a progressive liver disease, our data suggest that SIRT6 is involved in nearly all stages of NAFLD pathogenesis: from steatosis to inflammation and fibrosis. The major finding of this study is the characterization of the key role of SIRT6 in the regulation of TGFβ–SMAD3 signaling in HSCs. Initially, we set out to investigate the Sirt6 function in hepatocytes. Interestingly, our data have shown that Alb–Cre also leads to the *Sirt6* gene deletion in HSCs in addition to hepatocytes, although not as efficiently as in hepatocytes. Thus, we believe that the liver phenotype in our Alb–Cre–mediated Sirt6–KO mice is attributable to Sirt6 deficiency in both hepatocytes and HSCs. Previously, it has been shown that SIRT6 promotes hepatic triglyceride homeostasis through inhibition of de novo lipogenesis and activation of fatty acid oxidation by histone H3 deacetylation[14]; however, whether *Sirt6* is deleted or not in HSCs was not examined. SIRT6 also inhibits cholesterol biosynthesis by repression of the master regulator sterol regulatory element-binding protein 2 (SREBP2) and its target genes.[9] SIRT6 also represses the expression of the *PCSK9* gene to reduce the levels of low-density lipoprotein cholesterol.[8] Hepatic SIRT6 deficiency leads to increased cholesterol and triglyceride levels in the blood and liver as well.[8,9] Therefore, hepatic steatosis in Sirt6-KO mice is attributed mainly to Sirt6 deficiency in hepatocytes. With regard to liver fibrosis, Sirt6 function in HSCs plays a major role because the Sirt6 HSC-KO mice develop remarkable hepatic fibrosis after 4 weeks of Western diet feeding. It has been reported that the Alb–Cre–mediated *Sirt6* KO mice also developed NASH on a high-fat, high-fructose diet for 16 weeks.[20] Sirt6 expression in HSCs was not examined in that report. The investigators attributed the NASH phenotype in the *Sirt6* KO mice to the antioxidative stress function of Sirt6 by regulation of nuclear factor erythroid 2–related factor 2.[20] In this work, we used a different NASH diet that contains 20% kcal from protein, 40% kcal from carbohydrates (mainly corn

Figure 5. (*See previous page*). Sirt6 protects against diet-induced hepatic inflammation. (*A* and *B*) H&E, myeloperoxidase (MPO), and F4/80 staining and quantification analysis of liver sections of WT, Sirt6-KO, and Sirt6-Tg male mice fed with a WD for 4 weeks (n = 4). (*C–E*) Hepatic inflammatory gene expression and serum ALT in WT, Sirt6-KO, and Sirt6-Tg male mice fed with a WD for 4 weeks (n = 4). (*F*) Immunostaining and quantification of CK-19 in the liver sections of WT and Sirt6-KO mice fed with a WD for 4 weeks (n = 4). Data are presented as means ± SEM. $^{*}P < .05$, $^{**}P < .01$, and $^{***}P < .001$ for WD vs control for the same genotype; $^{\#}P < .05$, $^{\#\#}P < .01$, and $^{\#\#\#}P < .001$. CK-19, cytokeratin 19.

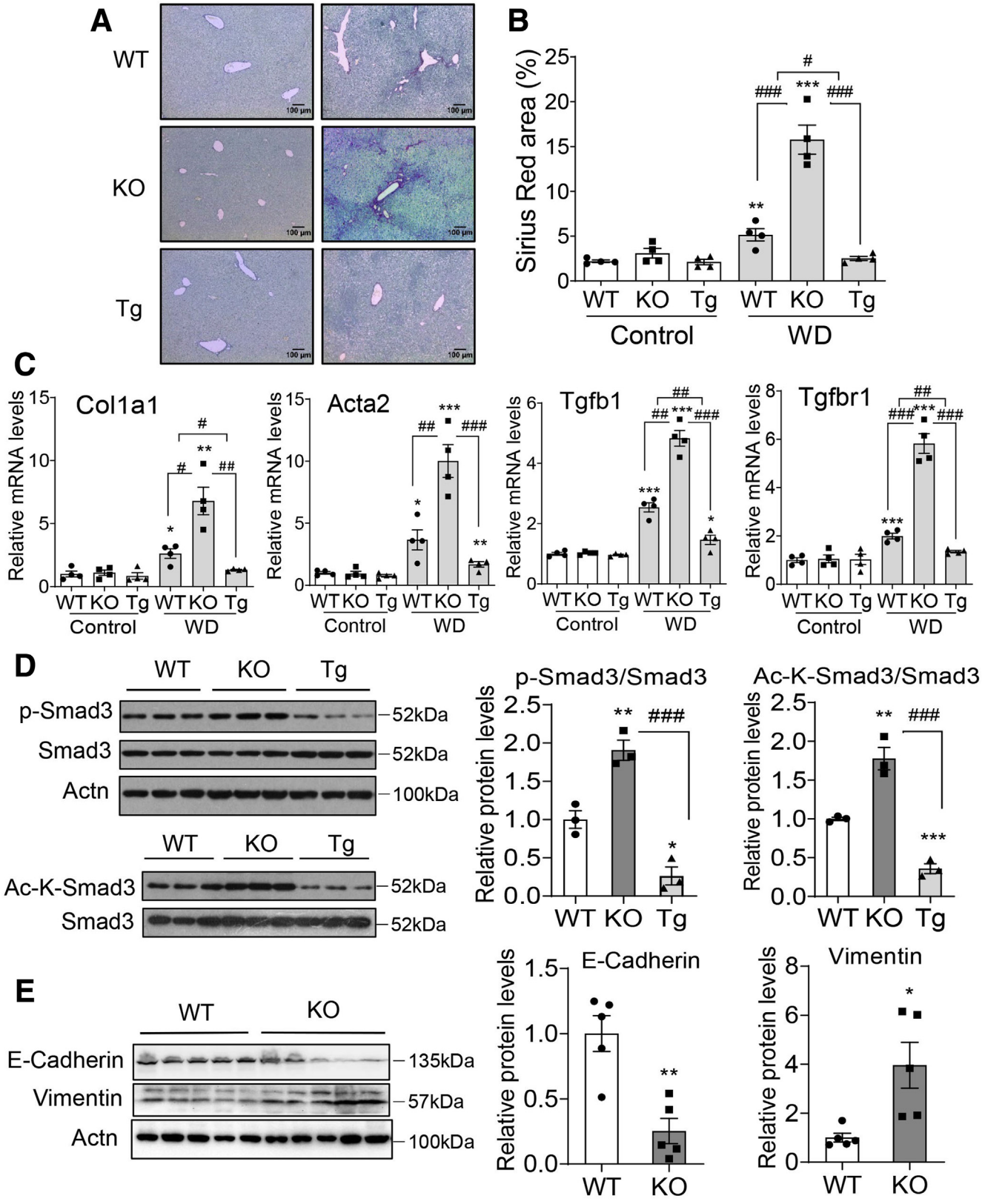

Figure 6. Sirt6 protects against diet-induced hepatic fibrosis. (*A* and *B*) Sirius Red staining of liver sections and quantification of the positive staining area in the livers of WT, Sirt6-KO, and Sirt6-Tg mice fed with a WD for 4 weeks (n = 4, 4- to 6-month-old males). (*C*) Real-time PCR analysis of fibrosis-related genes including *Col1a1*, *Acta2*, *Tgfb1*, and *Tgfbr1* in the livers of WT, Sirt6-KO, and Sirt6-Tg male mice fed with a WD for 4 weeks (n = 4). (*D*) Western blot analysis and quantification of Smad3, p-Smad3, and acetylated-Smad3 (Ac-K-Smad3) in the livers of WT, Sirt6-KO, and Sirt6-Tg mice. (*E*) Western blot analysis and quantification of E-cadherin and vimentin in the livers of WT and Sirt6-KO mice. Data are presented as means ± SEM. $^{*}P < .05$, $^{**}P < .01$, and $^{***}P < .001$ for WD vs control for the same genotype; $^{\#}P < .05$, $^{\#\#}P < .01$, and $^{\#\#\#}P < .001$. Actn, actinin; p-Smad, phospho-SMAD family member 2.

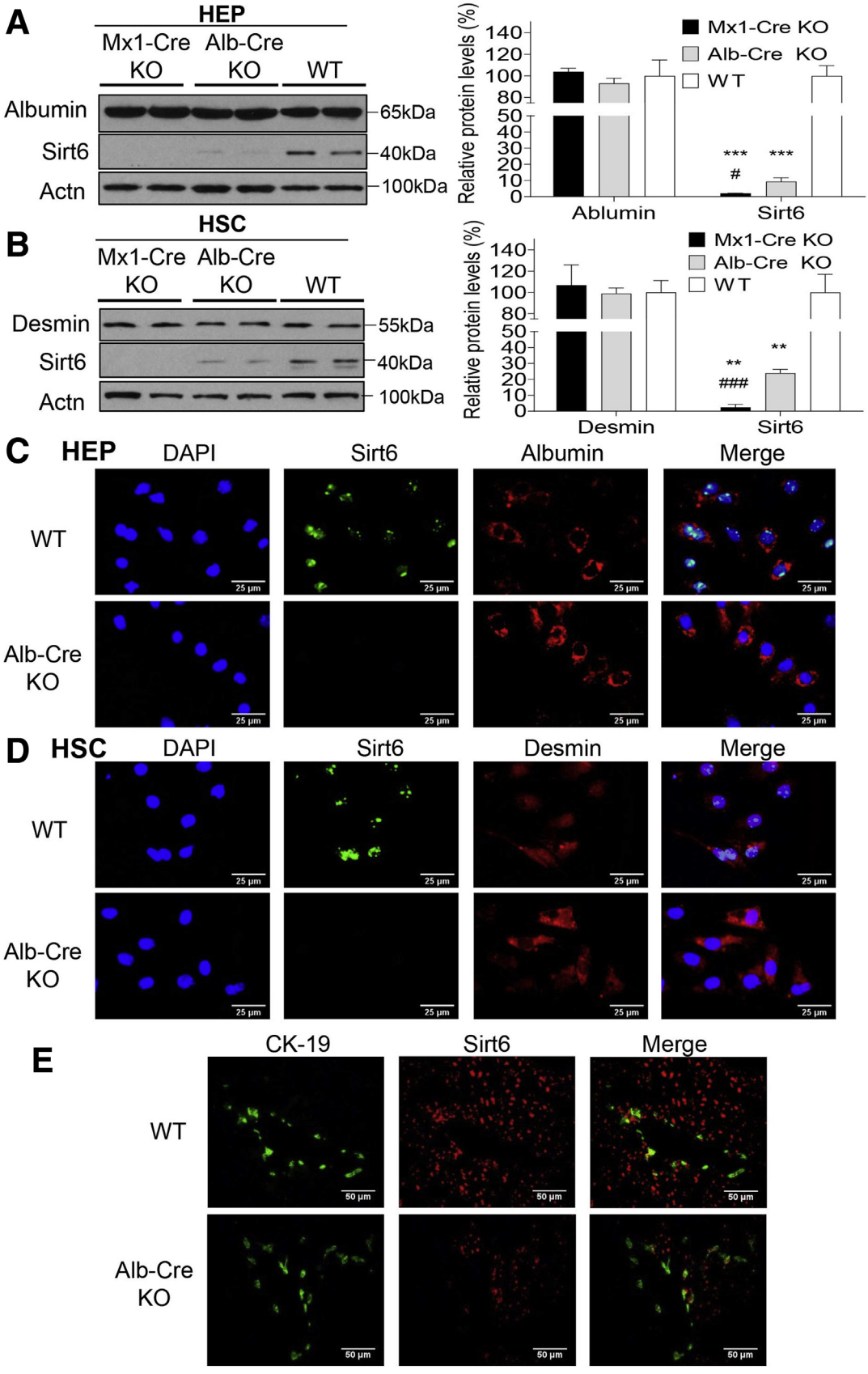
A
HEP
Mx1-Cre KO
Alb-Cre KO
WT
Albumin
Sirt6
Actn
65kDa
40kDa
100kDa
Relative protein levels (%)
Mx1-Cre KO
Alb-Cre KO
WT
Ablumin
Sirt6
B
HSC
Desmin
Sirt6
Actn
55kDa
40kDa
100kDa
Desmin
Sirt6
C
HEP
DAPI
Sirt6
Albumin
Merge
WT
Alb-Cre KO
D
HSC
DAPI
Sirt6
Desmin
Merge
WT
Alb-Cre KO
E
CK-19
Sirt6
Merge
WT
Alb-Cre KO

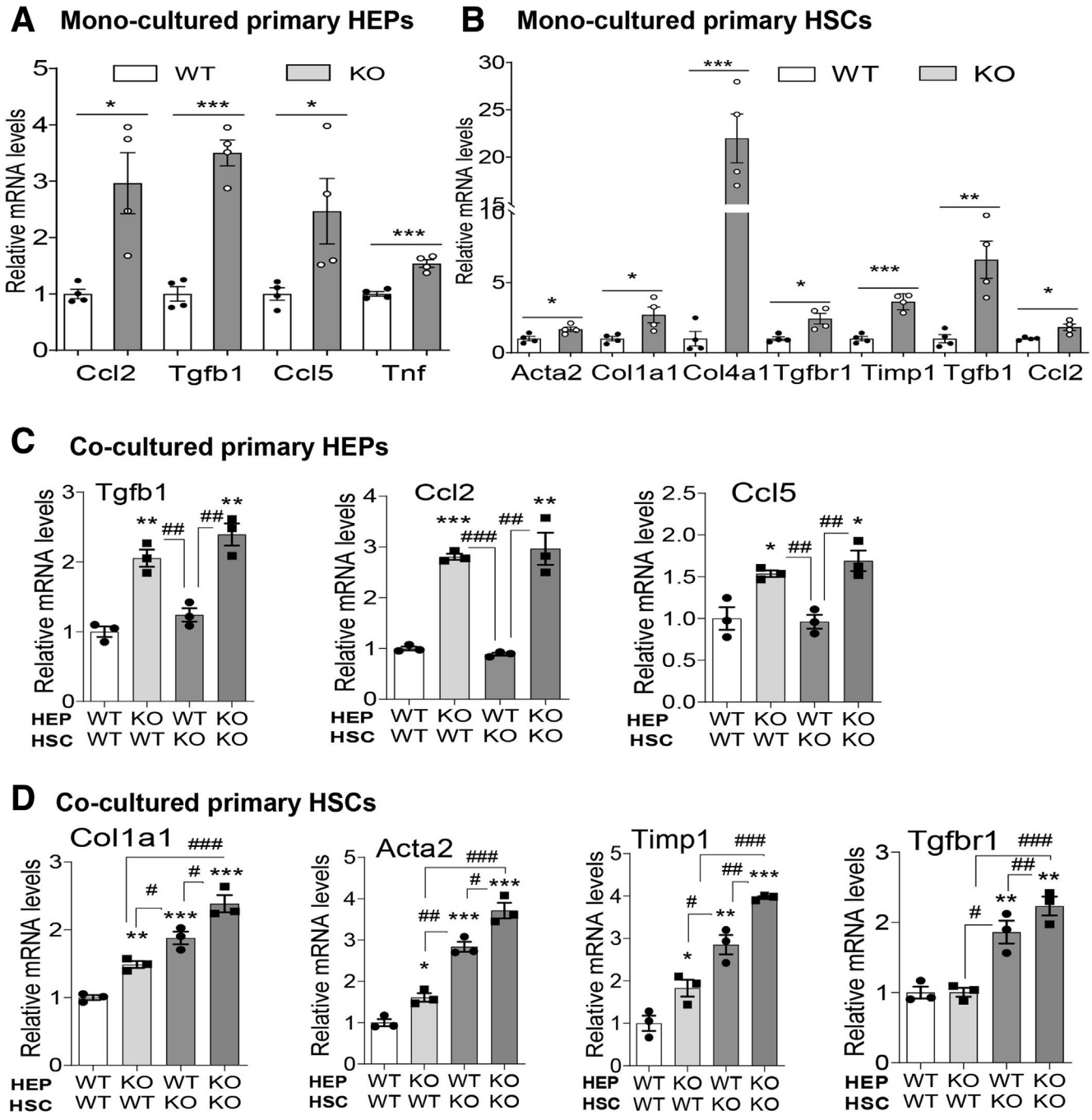

Figure 8. Gene expression analysis of Sirt6-deficient hepatocytes and HSCs. (*A–D*) Real-time PCR analysis of selected genes in monocultured or cocultured hepatocytes (HEPs) and HSCs. Data are presented as means ± SEM. $^{*}P < .05$, $^{**}P < .01$, and $^{***}P < .001$ vs WT or WT/WT; $^{\#}P < .05$, $^{\#\#}P < .01$, and $^{\#\#\#}P < .001$.

Figure 7. (*See previous page*). Alb–Cre leads to *Sirt6* gene deletion in both hepatocytes and HSCs in the Sirt6$^{f/f}$:Alb–Cre mouse liver. (*A* and *B*) Western blot and quantification analysis of Sirt6, albumin, and desmin in primary hepatocytes (HEPs) and HSCs from WT and Sirt6 KO mice induced by either Mx1–Cre or Alb–Cre. (*C*) Immunofluorescence microscopy analysis of Sirt6 and albumin in the WT and the Alb–Cre–mediated Sirt6-KO hepatocytes. (*D*) Immunofluorescence microscopy analysis of Sirt6 and desmin in the WT and the Alb–Cre–mediated Sirt6-KO HSCs. (*E*) Immunofluorescence microscopy analysis of Sirt6 and CK-19 in the WT and the Alb–Cre–mediated Sirt6-KO liver sections. Data are presented as means ± SEM. $^{**}P < .01$ and $^{***}P < .001$ vs WT; $^{\#}P < .05$ and $^{\#\#\#}P < .001$ for Alb-Cre KO vs Mx1–Cre KO. Actn, actinin; DAPI, 4′,6-diamidino-2-phenylindole; CK-19, cytokeratin 19.

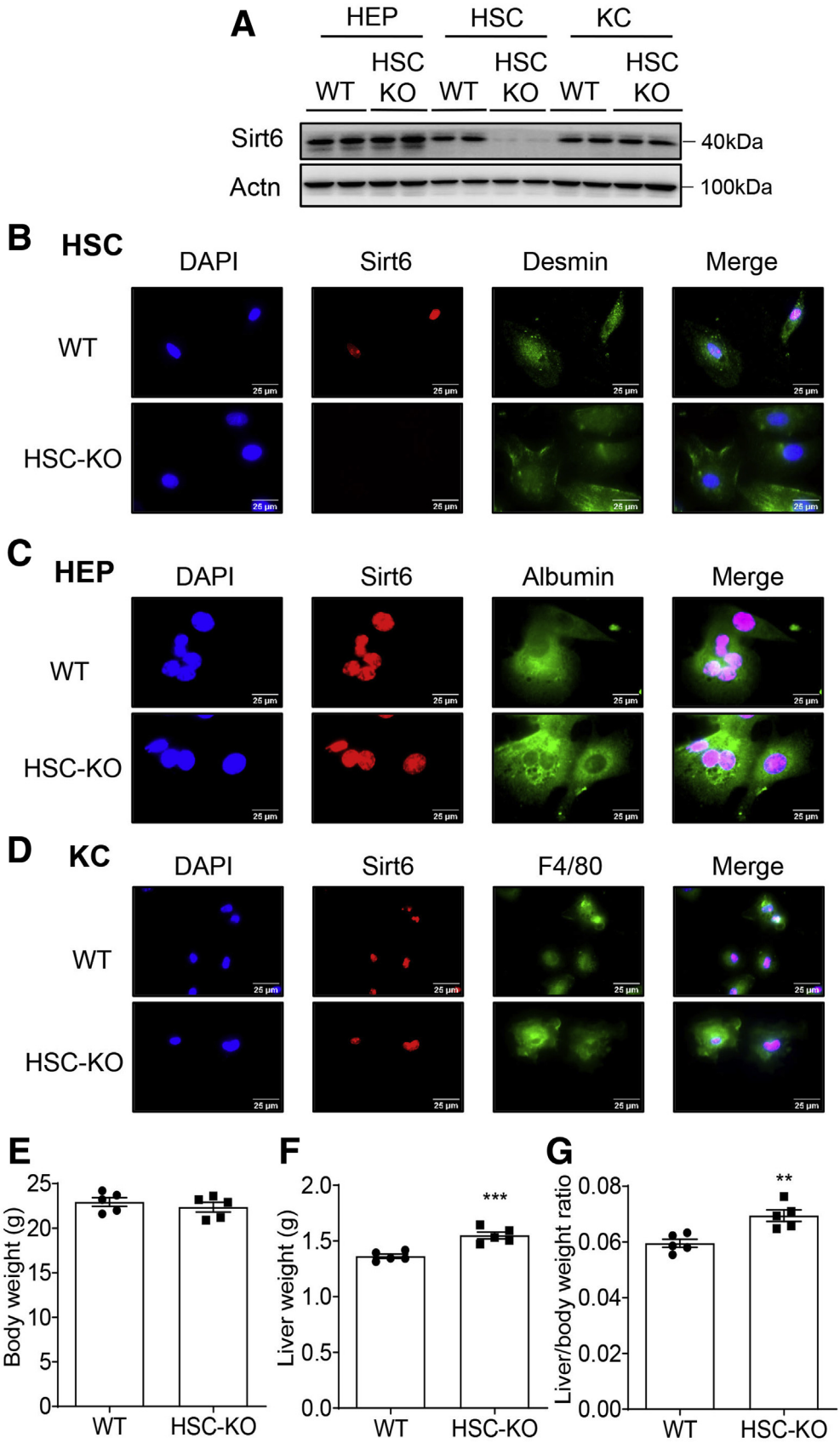

Figure 9. Characterization of HSC-specific *Sirt6* knockout mice. (*A*) Western blot analysis of Sirt6 protein in primary hepatocytes (HEPs), HSCs, and Kupffer cells (KCs) from WT and HSC-KO mice. (*B–D*) Immunofluorescence analysis of Sirt6 and cell-type–specific markers in HSCs, hepatocytes, and KCs isolated from WT and Lrat–Cre–mediated HSC-KO mice (n = 5, 3- to 4-month-old males). (*E–G*) Measurements of body and liver weights of WT and HSC-KO male mice (n = 5). Data are presented as means ± SEM. $^{**}P < .01$ and $^{***}P < .001$.

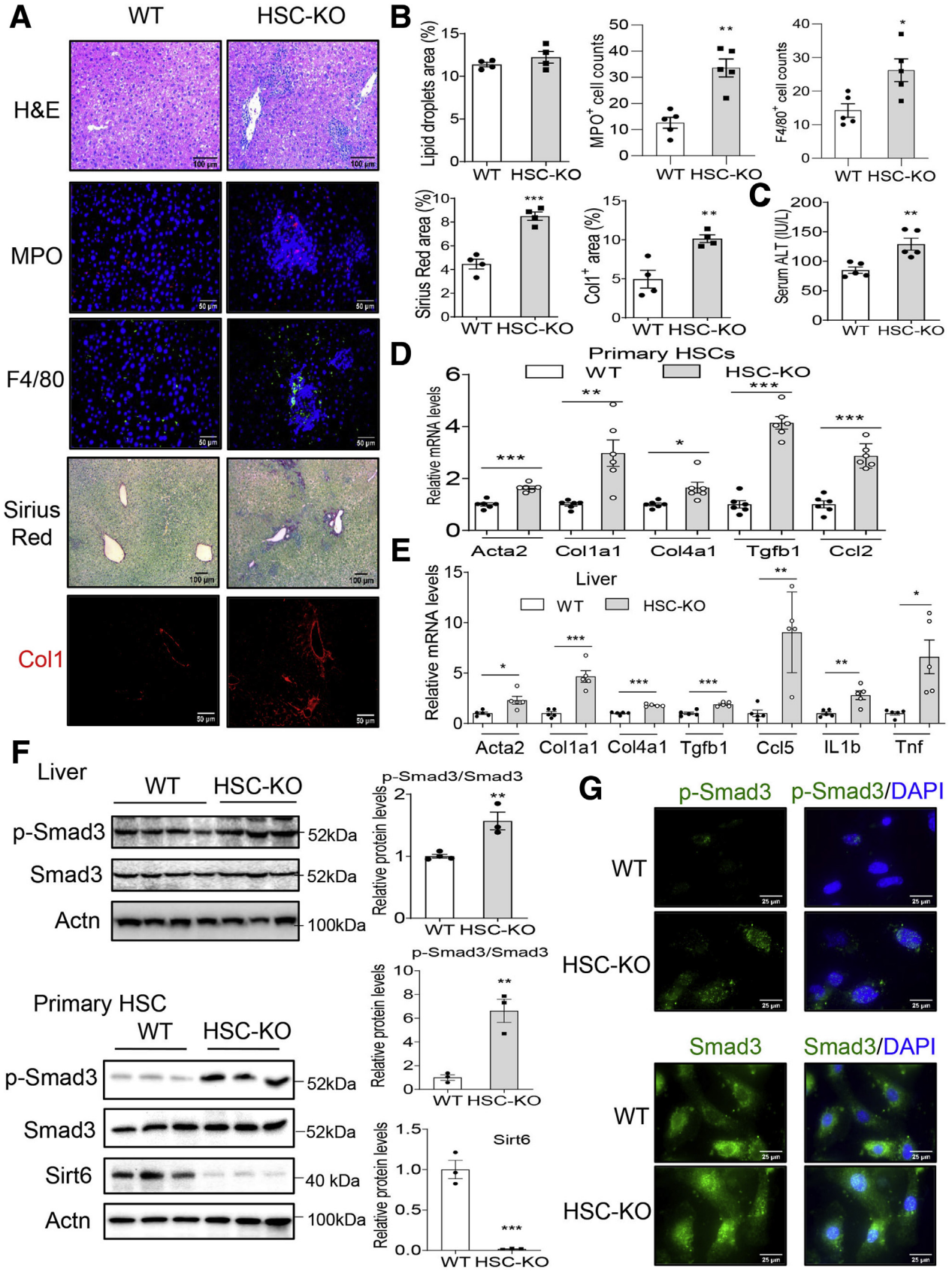
A
WT
HSC-KO
H&E
MPO
F4/80
Sirius Red
Col1
B
Lipid droplets area (%)
MPO+ cell counts
F4/80+ cell counts
Sirius Red area (%)
Col1+ area (%)
C
Serum ALT (IU/L)
D
Primary HSCs
Relative mRNA levels
Acta2
Col1a1
Col4a1
Tgfb1
Ccl2
E
Liver
Ccl5
IL1b
Tnf
F
Liver
p-Smad3
Smad3
Actn
52kDa
100kDa
p-Smad3/Smad3
Relative protein levels
Primary HSC
Sirt6
40 kDa
G
p-Smad3
p-Smad3/DAPI
Smad3
Smad3/DAPI

starch and sucrose), 40% kcal from fat (mainly cocoa butter), 1.25% cholesterol (by weight), and 0.5% sodium cholate (by weight), and treated mice for 4 to 8 weeks. On this diet, *Sirt6* KO mice developed the NASH phenotype more rapidly than with the high-fat, high-fructose diet used by the Park group.[20] Another reason why we chose to treat the WT and KO mice for 4 to 8 weeks but not much longer is because hepatic *Sirt6* gene expression is down-regulated rapidly by the NASH diet in WT mice. This down-regulation of *Sirt6* diminishes the gene knockout effect in the long term.

TGFβ is thought to be the most potent cytokine for the induction of hepatic fibrosis.[3] Although the canonical TGFβ–SMAD3 pathway has been well established, the mechanism of epigenetic regulation of SMAD3 activity remains incompletely understood, especially in HSCs. Previous reports have suggested that SIRT6 modulates the TGFβ–SMAD3 pathway[23–25]; however, HSC-specific SIRT6 function has not been investigated before. Our data suggest that SIRT6 is a key regulator of the SMAD3 transcriptional activity through deacetylation of SMAD3 and histone H3 lysine 9 in HSCs. SMAD3 can be acetylated at multiple lysine residues by p300/CREB binding protein (CBP).[5,45] Our data have shown that K333 and K378 of SMAD3 are major substrates of SIRT6. Deacetylation of either of them by SIRT6 has a significant negative effect on the SMAD3 transcriptional activity. Because the SMAD3 acetylation analysis was performed under Sirt6 gain-of-function and loss-of-function conditions, additional physiological conditions may be considered in future studies.

An excessive accumulation of hepatic lipids is believed to cause liver injury. This is also the case in animals with chronic WD feeding. Hepatic injury can trigger inflammation, as manifested by the increased numbers of macrophages and neutrophils in the Sirt6-deficient mouse livers. As a result, a number of inflammatory cytokine and chemokine genes, including *TNFα*, *TGFβ*, *IL1β*, *Ccl2*, and *Ccl5*, are activated. The resultant inflammatory microenvironment stimulates conversion of quiescent HSCs to activated HSCs (also known as *myofibroblasts*). The activated myofibroblasts produce excess collagen molecules to cause fibrosis. In addition, SIRT6-deficient myofibroblasts also lose the control of TGFβ gene regulation. This reinforces the vicious cycle of TGFβ → TGFβ receptor → SMAD3 → TGFβ.

The complete reversal of NASH in our Tg mice suggests that SIRT6 is a useful therapeutic target for NASH. Because the Sirt6 Tg mice used in this study were generated using the ubiquitous cytomegalovirus-Cre, additional characterization of other cell types in the liver including liver sinusoidal endothelial cells, cholangiocytes, Kupffer cells, and macrophages is needed to fully understand the cell-type–specific role of Sirt6 in the protection against NASH.

In summary, our data suggest that Sirt6 plays a critical role in HSCs by modulating the SMAD3 activity and histone H3 acetylation. Hepatic Sirt6 deficiency poses a high susceptibility to diet-induced NASH development. Modulation of Sirt6 activity can be a potential therapeutic strategy for NASH treatment.

Materials and Methods

Animals

All animal procedures performed in this work were approved by the Institutional Animal Care and Use Committee of Indiana University School of Medicine in accordance with the National Institutes of Health guidelines for the care and use of laboratory animals. Liver-specific *Sirt6* KO mice were generated by crossing *Sirt6* floxed mice with albumin-Cre Tg mice as previously described.[8,9,46] Inducible hepatic *Sirt6* gene knockout also was generated by crossing the *Sirt6* floxed mice with *Mx1*-Cre transgenic mice from the Jackson Laboratory (Bar Harbor, ME).[47] We confirmed the efficiency of deletion of the floxed *Sirt6* coding sequence in the $Sirt6^{f/f}$:Mx1-$Cre^{+/-}$ mouse liver after 3 intraperitoneal injections of polyinosinic:polycytidylic acid every other day, which induces an interferon response to activate expression of the Cre recombinase under the *Mx1* gene promoter. The induced ablation of hepatic *Sirt6* was nearly complete 10 days after the last polyinosinic:polycytidylic acid injection. *Sirt6* HSC-KO mice were generated by crossing the *Sirt6* floxed mice with *Lrat*-Cre mice.[48] *Sirt6* global Tg mice were generated by crossing an inducible *Sirt6* Tg mouse carrying a floxed transcriptional/translational stop (STOP) cassette at the Rosa 26 locus with a cytomegalovirus-Cre transgenic mouse from the Jackson Laboratory.[49] Animals were fed either a control diet (Teklad Diets 2018SX: 24% calories from protein, 18% calories from fat, and 58% calories from carbohydrate, Indianapolis, IN), or a WD (Research Diets D12109C, 20% calories from protein, 40% calories from fat, 40% calories from carbohydrate, and 1.25% cholesterol and 0.5% sodium cholate by weight, New Brunswick, NJ). Both males and females were used in the experiments and they were on the mixed background (C57BL/6J and 129/sv). At the end of the experiments, the animals were killed for blood and tissue collection.

Human Liver Specimens

Human liver samples were obtained from diagnosed NASH patients and control subjects. Paraffin-embedded

Figure 10. (***See previous page***). **HSC-specific *Sirt6* KO mice develop NASH.** (*A* and *B*) H&E, myeloperoxidase (MPO), F4/80, Sirius Red, and Col1 staining and quantification of liver sections of WT and HSC-KO mice (n = 5, 3- to 4-month-old males) fed with a WD for 4 weeks. (*C*) Serum ALT measurements of WT and HSC-KO male mice fed with a WD for 4 weeks (n = 5). (*D*) Real-time PCR analysis of selected genes in primary HSCs from WT and HSC-KO mice fed with a WD for 10 days (n = 3, 3-month-old males). (*E*) Real-time PCR analysis of selected genes in livers from WT and HSC-KO mice fed with a WD for 4 weeks. (*F* and *G*) Smad3 and p-Smad3 analyses (immunoblotting or fluorescence microscopy) in the livers of WT and HSC-KO male mice fed with a WD for 4 weeks and primary HSCs from WT and HSC-KO mice fed with a WD for 10 days. Data are presented as means ± SEM. $^{*}P < .05$, $^{**}P < .01$, and $^{***}P < .001$ vs WT. DAPI, 4′,6-diamidino-2-phenylindole; p-Smad3, phospho-SMAD family member 3.

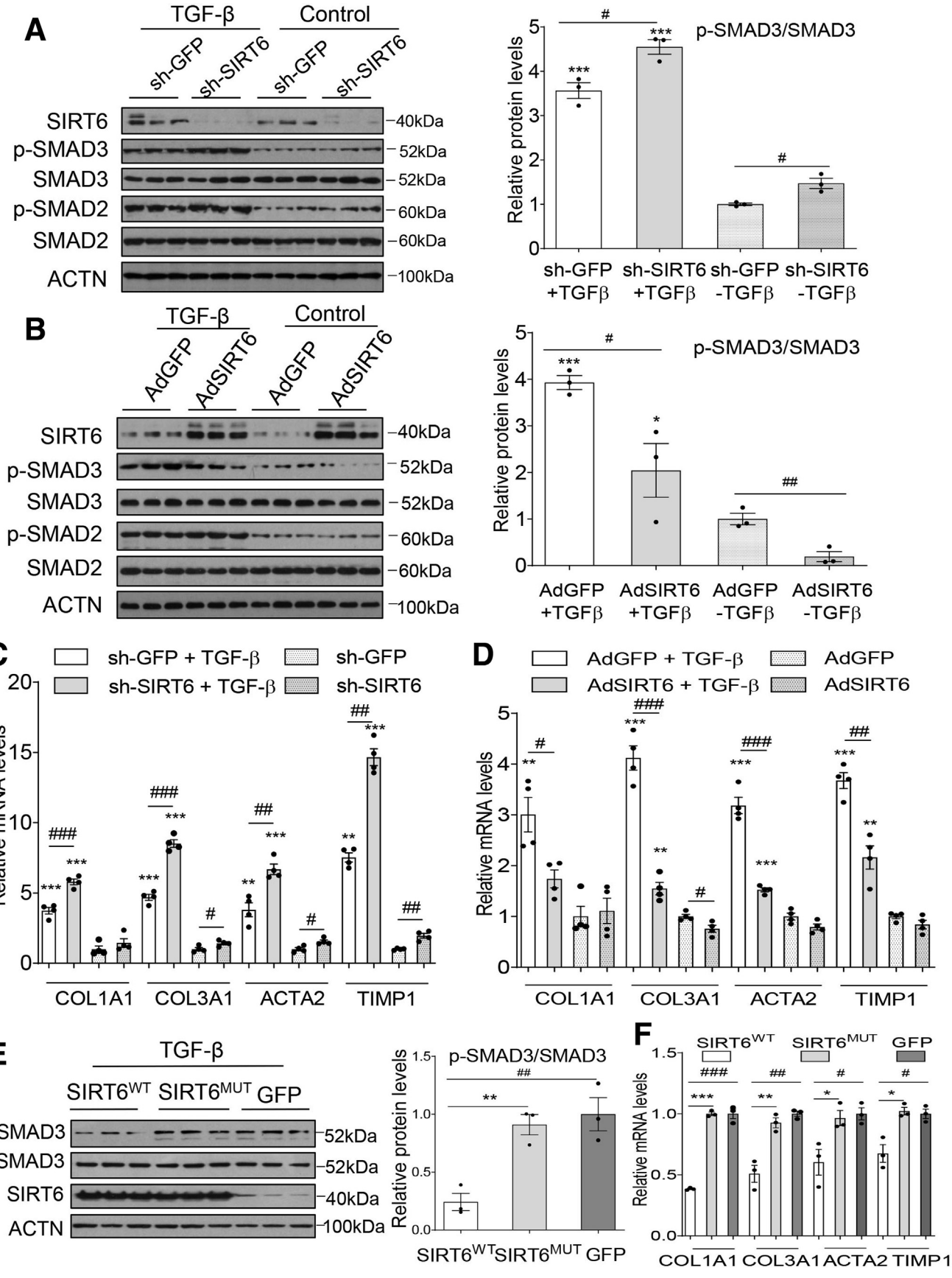
A
TGF-β
Control
sh-GFP
sh-SIRT6
sh-GFP
sh-SIRT6
SIRT6
p-SMAD3
SMAD3
p-SMAD2
SMAD2
ACTN
40kDa
52kDa
52kDa
60kDa
60kDa
100kDa
p-SMAD3/SMAD3
Relative protein levels
sh-GFP +TGFβ
sh-SIRT6 +TGFβ
sh-GFP -TGFβ
sh-SIRT6 -TGFβ
B
TGF-β
Control
AdGFP
AdSIRT6
AdGFP
AdSIRT6
SIRT6
p-SMAD3
SMAD3
p-SMAD2
SMAD2
ACTN
40kDa
52kDa
52kDa
60kDa
60kDa
100kDa
p-SMAD3/SMAD3
Relative protein levels
AdGFP +TGFβ
AdSIRT6 +TGFβ
AdGFP -TGFβ
AdSIRT6 -TGFβ
C
sh-GFP + TGF-β
sh-SIRT6 + TGF-β
sh-GFP
sh-SIRT6
Relative mRNA levels
COL1A1
COL3A1
ACTA2
TIMP1
D
AdGFP + TGF-β
AdSIRT6 + TGF-β
AdGFP
AdSIRT6
Relative mRNA levels
COL1A1
COL3A1
ACTA2
TIMP1
E
TGF-β
SIRT6WT
SIRT6MUT
GFP
p-SMAD3
SMAD3
SIRT6
ACTN
52kDa
52kDa
40kDa
100kDa
p-SMAD3/SMAD3
Relative protein levels
SIRT6WT
SIRT6MUT
GFP
F
SIRT6WT
SIRT6MUT
GFP
Relative mRNA levels
COL1A1
COL3A1
ACTA2
TIMP1

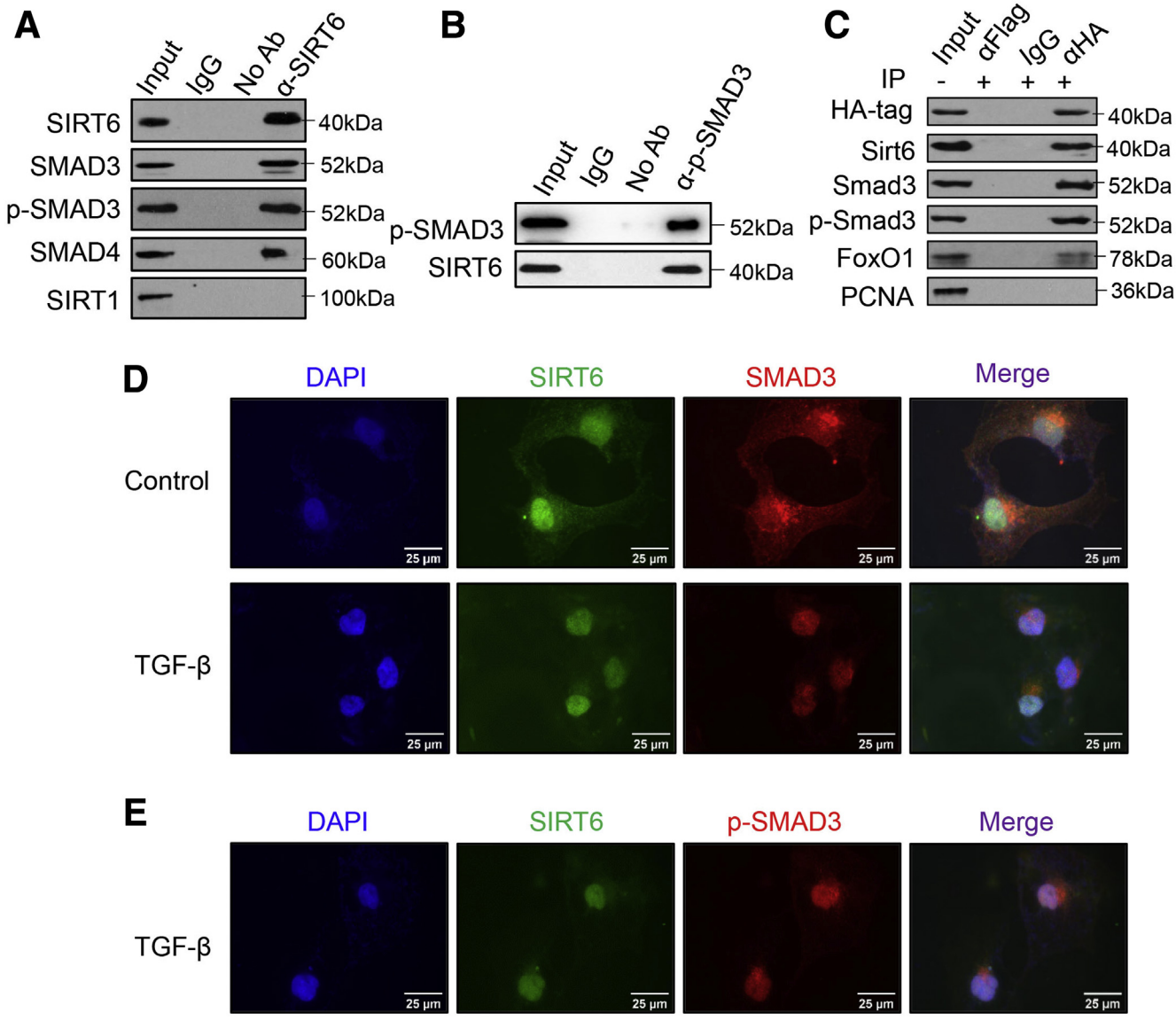

Figure 12. SIRT6 interacts with SMAD3 in hepatic stellate cells. (*A* and *B*) Co-immunoprecipitation analysis of interactions between the endogenous SIRT6 and SMAD3 or p-SMAD3 in LX-2 cells in the presence of TGFβ1 (5 ng/mL) for 24 hours. (*C*) Co-immunoprecipitation analysis of interactions between Sirt6 and Smad3/p-Smad3 in the livers of Sirt6 transgenic mice fed with a WD for 4 weeks. (*D*) Immunofluorescence microscopy of SIRT6 and SMAD3 in LX-2 cells in the absence or presence of TGFβ1 (5 ng/mL) for 3 hours. (*E*) Immunofluorescence microscopy of SIRT6 and p-SMAD3 in LX-2 cells in the presence of TGFβ1 (5 ng/mL) for 3 hours. Ab, antibody; DAPI, 4′,6-diamidino-2-phenylindole; Flag, FLAG tag; HA, hemagglutinin; IP, immunoprecipitation; PCNA, proliferating cell nuclear antigen; p-SMAD3, phospho-SMAD family member 3.

Figure 11. (***See previous page***). **SIRT6 suppresses the TGFβ–SMAD3 pathway in HSCs.** (*A*) Western blot analysis and quantification of SMAD3 and p-SMAD3 in LX-2 cells that were transduced with adenoviral GFP or SIRT6 shRNA (sh-GFP or sh-SIRT6) in the absence or presence of TGFβ1 (5 ng/mL) for 24 hours. (*B*) Western blot analysis and quantification of SMAD3 and p-SMAD3 in LX-2 cells that were transduced with adenoviral GFP or SIRT6 (AdGFP or AdSIRT6) in the absence or presence of TGFβ1 (5 ng/mL) for 24 hours. (*C* and *D*) Real-time PCR analysis of selected fibrosis genes in LX-2 cells that were transduced with adenoviral sh-GFP, sh-SIRT6, AdGFP, or AdSIRT6 in the absence or presence of TGF-β1 (5 ng/mL) for 24 hours. (*E* and *F*) Western blot analysis of SMAD3 and p-SMAD3 and real-time PCR analysis of selected fibrosis genes in LX-2 cells that were transfected with wild-type SIRT6, SIRT6 (H133Y) mutant, or GFP in the presence of TGFβ1 (5 ng/mL) for 24 hours. Data are presented as means ± SEM. $^{*}P < .05$, $^{**}P < .01$, and $^{***}P < .001$ for TGFβ1 treatment vs control for the same protein or gene; $^{\#}P < .05$, $^{\#\#}P < .01$, and $^{\#\#\#}P < .001$. ACTN, actinin; AdGFP, adenoviral green fluorescent protein; GFP, green fluorescent protein; p-SMAD3, phospho-SMAD family member 3.

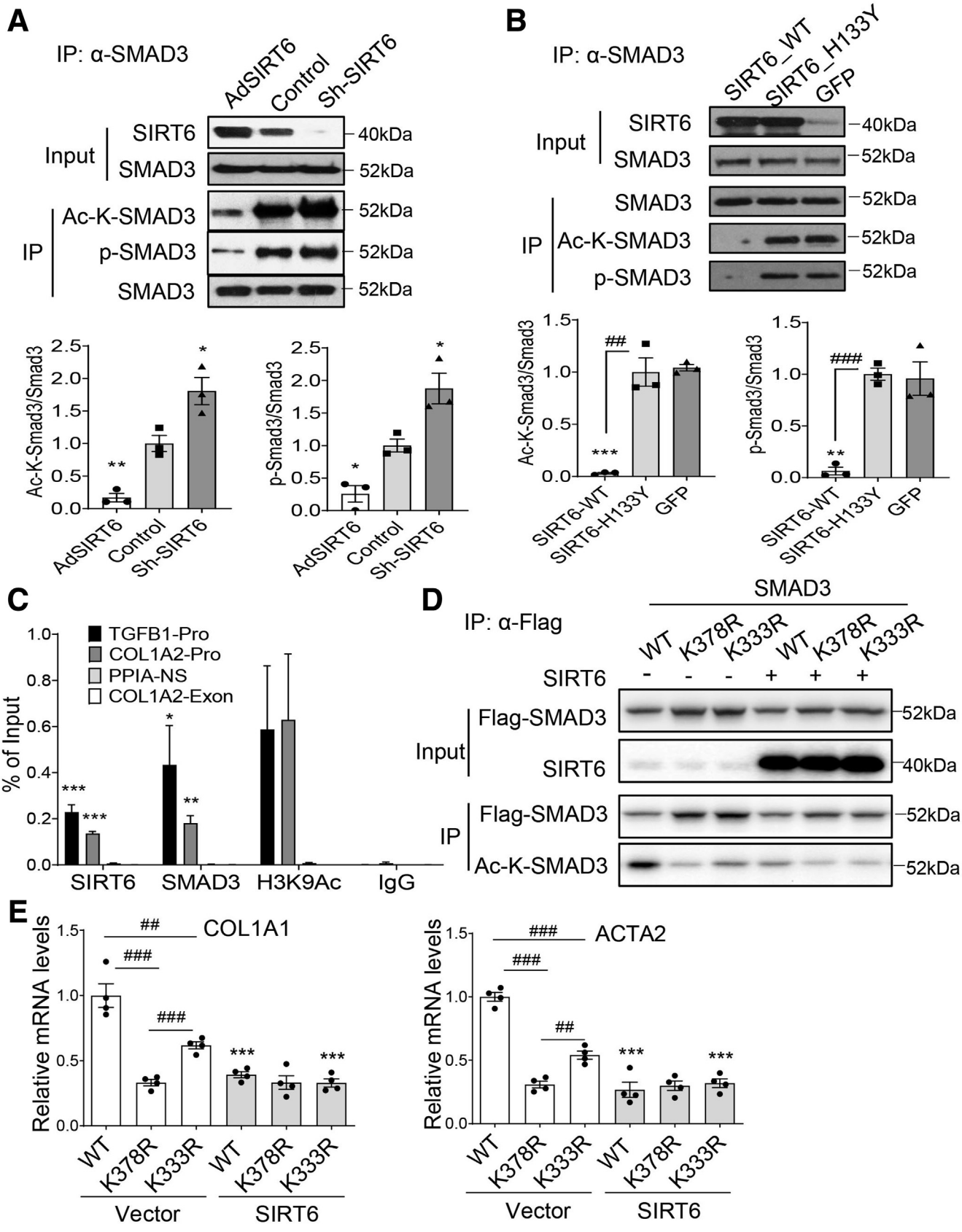
A
IP: α-SMAD3
AdSIRT6
Control
Sh-SIRT6
Input
SIRT6
SMAD3
IP
Ac-K-SMAD3
p-SMAD3
SMAD3
40kDa
52kDa
Ac-K-Smad3/Smad3
p-Smad3/Smad3
B
IP: α-SMAD3
SIRT6_WT
SIRT6_H133Y
GFP
SIRT6-WT
SIRT6-H133Y
C
TGFB1-Pro
COL1A2-Pro
PPIA-NS
COL1A2-Exon
% of Input
SIRT6
SMAD3
H3K9Ac
IgG
D
IP: α-Flag
SMAD3
WT
K378R
K333R
Flag-SMAD3
E
Relative mRNA levels
COL1A1
ACTA2
Vector
SIRT6

Table 1. Demographic and Pathologic Characteristics of Patients With NASH

ID	Age, *y*	Sex	Steatosis	Ballooning	Lobular inflammation	NAS score
1	68	F	1	2	2	5
2	49	F	1	2	1	4
3	56	M	1	2	1	4
4	51	F	2	1	1	4
5	58	F	3	1	1	5
6	56	M	2	1	1	4
7	48	F	3	1	1	5
8	57	F	2	1	1	4
9	62	F	1	2	1	5
10	53	F	2	2	1	5
11	44	F	1	0	1	2
12	64	M	1	0	1	2

NAS, NAFLD activity score.

liver sections from patients with simple steatosis and different stages of fibrosis by histopathologic diagnosis of NASH were obtained under the institutional review board–approved protocol at the Indiana University–Purdue University Indianapolis. General characteristics of the NASH patients are described in Table 1.

Plasmid Constructs and Adenoviral Vectors

Human SIRT6 and SIRT6 H133Y mutant (catalytically inactive) and green fluorescent protein (GFP) coding sequences were cloned into a pcDNA3 plasmid vector (Invitrogen, Carlsbad, CA) with a FLAG epitope or hemagglutinin (HA) epitope tag. SIRT6 and GFP overexpression adenoviruses were prepared in an AdEasy adenoviral vector system (Agilent, Santa Clara, CA) following the manufacturer's manual. SIRT6 and GFP shRNA adenoviruses were made using a BLOCK-iT system (Invitrogen). Human SMAD3 lysine acetylation sites were mutated using a Q5 site-directed mutagenesis kit (New England Biolabs, Ipswich, MA). DNA oligonucleotides used in this work are described in Table 2. The recombinant DNA work was approved by the Indiana University Institutional Biosafety Committee.

Cell Culture, Plasmid Transfection, and Adenoviral Transduction

Human hepatic stellate cell line LX-2 (MilliporeSigma, Burlington, MA) was cultured in Dulbecco's modified Eagle medium (DMEM) (Thermo Fisher Scientific, Waltham, MA) supplemented with 2% fetal bovine serum and penicillin/streptomycin (Thermo Fisher Scientific). For adenoviral transduction, we used a multiplicity of infection of 20 for overexpression and a multiplicity of infection of 100 for shRNA knockdown experiments. Mouse primary cells were isolated from WT, Sirt6-KO (Alb-Cre), Sirt6-KO (Mx1-Cre), and HSC-KO (Lrat-Cre) mice. Hepatocytes, Kupffer cells, and HSCs were isolated as previously described.[50] Experiments were performed from 3–4 mice per genotype. To set up co-culture of hepatocytes and HSCs, freshly isolated primary mouse hepatocytes were seeded in a Transwell insert at 0.5×10^6/well with DMEM plus 10% fetal bovine serum, and primary mouse HSCs were seeded in a well of a Transwell plate at 0.5×10^6/well with DMEM plus 10% fetal bovine serum.

Real-Time PCR Analysis

Total RNAs were isolated from cells or tissues using the TRI reagent (MilliporeSigma) and converted into complementary DNA using a complementary DNA synthesis kit (Applied Biosystems, Foster City, CA). Real-time PCR analysis was performed using SYBR Green Master Mix (Promega, Madison, WI) in an Realplex PCR system (Eppendorf North America, Hauppauge, NY). Transcript levels were analyzed with the $2^{-\text{delta delta cycle threshold}}$ method, and quantification was normalized to the internal

Figure 13. (***See previous page***). **SIRT6 attenuates the SMAD3 transcriptional activity via deacetylation.** (*A* and *B*) SMAD3 acetylation and phosphorylation and quantification analysis in LX-2 cells either transduced with adenoviral Sirt6 (AdSirt6), Sirt6 shRNA (sh-Sirt6) sh-Sirt6, or green fluorescent protein shRNA (shGFP) adenoviruses, or transfected with SIRT6_WT, Sirt6_H133Y mutant, or GFP plasmids. (*C*) ChIP-PCR analysis of chromatin binding of SIRT6 and SMAD3 in the indicated gene regions in LX-2 cells in the presence of TGFβ1 (5 ng/mL) for 24 hours using specific antibodies against SIRT6, SMAD3, and H3K9Ac, or IgG control. The chromatin binding activity of SIRT6, SMAD3 and H3K9Ac is presented as the percentage of the input DNA amount. (*D* and *E*) Western blot analysis of deacetylation of WT or mutant SMAD3 by SIRT6 and real-time PCR analysis of the deacetylation effect on fibrosis genes in LX-2 cells. Data are presented as means ± SEM. $^{*}P < .05$, $^{**}P < .01$, and $^{***}P < .001$ vs (*A*) control or GFP, (*C*) PPIA-non-specific (NS), or (*E*) vector for the same SMAD3 genotype; $^{\#\#}P < .01$ and $^{\#\#\#}P < .001$. Ad, adenoviral; Flag, FLAG tag; IP, immunoprecipitation; Pro, promoter; p-SMAD3, phospho-SMAD family member 3.

Table 2. DNA Oligonucleotide Sequences

Name	Sequence
Mouse *Sirt6* qPCR	Forward: 5'-ACGTCAGAGACACGGTTGTG-3' Reverse: 5'-CCTCTACAGGCCCGAAGTC-3'
Mouse *Tnf* qPCR	Forward: 5'-GGCCTCCCTCTCATCAGTTC-3' Reverse: 5'-CACTTGGTGGTTTGCTACGA-3'
Mouse *Il1b* qPCR	Forward: 5'-TGTGAAATGCCACCTTTTGA-3' Reverse: 5'-GGTCAAAGGTTTGGAAGCAG-3'
Mouse *Col1a1* qPCR	Forward: 5'-CACCTGGTCCACAAGGTTTC-3' Reverse: 5'-CCCATCATCTCCATTCTTGC-3'
Mouse *Col3a1* qPCR	Forward: 5'-TGCTGGAAAGGATGGAGAGT-3' Reverse: 5'-TGGGCCTTTGATACCTGGAG-3'
Mouse *Col4a1* qPCR	Forward: 5'-TTCGCCTCCAGGAACGACTA-3' Reverse: 5'-AAACCGCACACCTGCTAATG-3'
Mouse *Acta2* qPCR	Forward: 5'-AGGCACCACTGAACCCTAAG-3' Reverse: 5'-GACAGCACAGCCTGAATAGC-3'
Mouse *Tgfb1* qPCR	Forward: 5'-CGCAACAACGCCATCTATGA-3' Reverse: 5'-ACTGCTTCCCGAATGTCTGA-3'
Mouse *Timp1* qPCR	Forward: 5'-CATGGAAAGCCTCTGTGGAT-3' Reverse: 5'-CTCAGAGTACGCCAGGGAAC-3'
Mouse *Tgfbr1* qPCR	Forward: 5'-TTCCTCGAGACAGGCCATTTG-3' Reverse: 5'-CAGCTGACTGCTTTTCTGTAGT-3'
Mouse *Ccl2* qPCR	Forward: 5'-CCCAATGAGTAGGCTGGAGA-3' Reverse: 5'-TCTGGACCCATTCCTTCTTG-3'
Mouse *Ccl5* qPCR	Forward: 5'-GTGCCCACGTCAAGGAGTAT-3' Reverse: 5'-CTCTGGGTTGGCACACACTT-3'
Mouse *Il6* qPCR	Forward: 5'-CAAAGCCAGAGTCCTTCAGAG-3' Reverse: 5'-GAGCATTGGAAATTGGGGTA-3'
Mouse *Arg1* qPCR	Forward: 5'-CAAGACAGGGCTCCTTTCAG-3' Reverse: 5'-TGAGTTCCGAAGCAAGCCAA-3'
Mouse *Il10* qPCR	Forward: 5'-CAGAGCCACATGCTCCTAGA-3' Reverse: 5'-GCTTGGCAACCCAAGTAACC-3'
Human *COL1A1* qPCR	Forward: 5'-CCCGAGGCTCTGAAGGTC-3' Reverse: 5'-GAGCACCATTGGCACCTTT-3'
Human *COL3A1* qPCR	Forward: 5'-GCAGGGTCTCCTGGTTCAAA-3' Reverse: 5'-CGGGACCCATTTCGCCTTTA-3'
Human *ACTA2* qPCR	Forward: 5'-CCGGGACTAAGACGGGAATC-3' Reverse: 5'-TTGTCACACACCAAGGCAGT-3'
Human *TIMP1* qPCR	Forward: 5'-TTTTGTGGCTCCCTGGAACA-3' Reverse: 5'-AAACAGGGAAACACTGTGCAT-3'
Human *SMAD3* K333R mutation PCR	Forward: 5'-ACCGTCTGCAGGATCCCACCAGG-3' Reverse: 5'-GGCCGGGTGCCAGCCATA-3'
Human *SMAD3* K378R mutation PCR	Forward: 5'-AGCTTCGTCAGAGGCTGGGGA-3' Reverse: 5'-CATGCGGATGGTGCACATTC-3'
Human *TGFB1* gene promoter ChIP PCR	Forward: 5'-ACGTCAGAGACACGGTTGTG-3' Reverse: 5'-AGGGTGTCAGTGGGAGGA-3'
Human *COL1A2* gene promoter ChIP PCR	Forward: 5'-ACTCCGACGTGTCCCATAGTG-3' Reverse: 5'-GGCTGGCTTCTTAAATTGGTTCCA-3'
Human *PPIA* gene promoter ChIP PCR	Forward: 5'-CTAAAGCGCCAGGTATGAGCA-3' Reverse: 5'-GCGAATTTCTTCAGGCAAAG-3'
Human *COL1A2* gene exon ChIP PCR	Forward: 5'-CCATCACGCCTGCCCTTC-3' Reverse: 5'-CAGACTGGGCCAATGTCCAC-3'
Human *SIRT6* AdEasy primers	Forward: 5'-CTTCCGATATCGCCACCATGTCGGTGAATTACGCGGC-3' Reverse: 5'-AAGGAACTCGAGGCTGGGGACCGCCTTG-3'
Human *SIRT6* shRNA target	5'-GCTACGTTGACGAGGTCATGA-3'
GFP control shRNA	5'-GCATCAAGGTGAACTTCAAGA-3'

qPCR, quantitative polymerase chain reaction.

Table 3. Antibody information

Antibody	Source	Catalog Number	Application
Sirt6	Cell Signaling Technology, Danvers, MA	12486S	WB: 1:1000 IP: 1 μg CHIP: 4 μg
Sirt6	Sigma, St. Louis, MO	S4197	IF: 1:200
Sirt6	Novus, Centennial, CO	NB1002522	IF: 1:200
Sirt6	Invitrogen, Waltham, MA	MA5-24768	IF: 1:200
α-Actinin	Santa Cruz Biotechnology, Dallas, TX	sc-17829	WB: 1:10000
Smad3	Cell Signaling Technology	9523S	WB: 1:1000 IF: 1:200 IP: 1 μg CHIP: 4 μg
Phospho-Smad3 (Ser423/425)	Cell Signaling Technology	9520S	WB: 1:1000 IF: 1:200 IP: 1 μg
Anti-HA agarose	Thermo Fisher Scientific, Waltham, MA	26181	IP: 20 μL
Anti-Flag gel	Sigma	A2220	IP: 20 μL
Protein A/G Plus Agarose	Santa Cruz Biotechnology	Sc-2003	IP: 20 μL
Anti-HA	Cell Signaling Technology	3724S	WB: 1:3000
FoxO1	Cell Signaling Technology	2880	WB: 1:1000
PCNA	Cell Signaling Technology	2586S	WB: 1:1000
E-cadherin	Cell Signaling Technology	3195S	WB: 1:1000
Vimentin	Cell Signaling Technology	5741S	WB: 1:1000
Desmin	Thermo Fisher Scientific	RB-9014-P	WB: 1:1000 IF: 1:100
Desmin	DSHB, Iowa City, IA	D3	IF: 1:25
CK-19	DSHB	TROMA-III	IF: 1:25
Albumin	Santa Cruz Biotechnology	Sc-271605	WB: 1:1000 IF: 1:100
Smad2	Cell Signaling Technology	5339S	WB 1:1000
Phospho-Smad2 (Ser465/467)	Cell Signaling Technology	18338S	WB: 1:1000
Anti-Flag	Sigma	F1804	WB: 1:3000
Sirt1	Cell Signaling Technology	8469S	WB: 1:1000
Smad4	Cell Signaling Technology	46535S	WB: 1:1000
Acetylated-lysine	Cell Signaling Technology	9441L	WB: 1:1000
Normal mouse IgG	Invitrogen	10400C	IP: 1 μg
Normal rabbit IgG	Invitrogen	10500C	IP: 1 μg
MPO	Invitrogen	PA516672	IHC: 1:100
F4/80	Invitrogen	MA516363	IHC: 1:100 IF: 1:100
Collagen I	Abcam, Cambridge, MA	ab21286	IF: 1:100

CK-19, cytokeratin 19; Flag, FLAG tag; HA, hemagglutinin tag; IF, immunofluorescence; IHC, immunohistochemistry; IP, immunoprecipitation; MPO, myeloperoxidase; PCNA, proliferating cell nuclear antigen; WB, Western blotting.

control gene *PPIA*. Primer sequences of the genes used in this work are described in Table 2.

Blood Chemistry and Metabolic Analysis

Lipids were extracted from tissues using a chloroform–methanol extraction protocol as previously described.[51] Triglyceride measurements were performed using an L-type triglyceride assay kit (FUJIFILM Wako Diagnostics, Richmond, VA). Serum ALT analysis was performed using an assay kit from Thermo Fisher Scientific.

Immunocytochemistry and Immunohistochemistry Analysis

Cells were grown in a glass-bottom dish and then fixed with 4% paraformaldehyde for 15 minutes at room temperature, followed by washing 3 times with phosphate-

buffered saline (PBS), and incubating overnight with primary antibodies as described in Table 3. After washing 3 times with PBS, cells were incubated with Alexa Fluor–conjugated secondary antibodies (1:250; Invitrogen) for 1.5 hours, followed by counterstaining and mounting with Prolong Gold antifade mountant with 4′,6-diamidino-2-phenylindole (Invitrogen). Images were taken with a Zeiss Axio Observer Z1 fluorescent microscope (Zeiss USA, Thornwood, NY). Liver tissue samples were fixed in 10% formalin solution and stored in 70% ethanol before they were processed for embedding and sectioning at the Histology Core of Indiana University School of Medicine. Liver sections were stained with H&E or Sirius Red stain (MilliporeSigma). Immunohistochemistry analysis was performed for myeloperoxidase, F4/80, and other proteins using the following procedures. Liver sections were deparaffinized and hydrated in 1 mmol/L EDTA buffer for antigen retrieval at 100°C for 5 minutes, and the liver sections then were incubated with normal horse serum for 1 hour. Next, the liver sections were incubated with primary antibodies described in Table 3 at 4°C overnight. After they were washed with PBS containing 0.05% Tween-20, the liver sections were incubated with either a biotinylated universal pan-specific antibody included in a Vectastain ABC kit from Vector Laboratories (Burlingame, CA) or fluorophore-conjugated secondary antibody for 2 hours. The sections incubated with the biotinylated antibody subsequently were incubated with avidin–biotin peroxidase complexes (Vector Laboratories) for 1 hour. Peroxidase activity was detected using diaminobenzidine solution (Vector Laboratories). Images were taken using a regular microscope (original magnification, 100× or 200×; Leica, Buffalo Grove, IL) or a fluorescent microscope (original magnification, 200×, 400×, or 630×; Zeiss USA). Quantification of the images was performed from randomly selected sections of at least 5 fields of each sample using ImageJ software (version 1.52; National Institutes of Health, Bethesda, MD).

Western Blot and Immunoprecipitation Analyses

Immunoblotting and immunoprecipitation analyses were performed as previously described.[52] Tissue samples were homogenized in the lysis buffer (50 mmol/L HEPES, pH 7.5, 150 mmol/L NaCl, 10% glycerol, 1% Triton X-100, 1.5 mmol/L $MgCl_2$, 1 mmol/L EDTA, 10 mmol/L sodium pyrophosphate, 100 mmol/L sodium fluoride, and freshly added 100 μmol/L sodium vanadate, 1 mmol/L phenylmethylsulfonyl fluoride, and 1× cOmplete protease inhibitor cocktail [Roche, Indianapolis, IN]). Cell lysates were prepared in the NP-40 lysis buffer (1% NP-40, 20 mmol/L Tris, pH 7.4, 137 mmol/L NaCl, 2 mmol/L EDTA, 10% glycerol, 1 mmol/L phenylmethylsulfonyl fluoride, and 1× cOmplete protease inhibitor cocktail). Protein samples were resolved by sodium dodecyl sulfate–polyacrylamide gel electrophoresis and transferred to a nitrocellulose membrane for immunoblotting analysis using specific antibodies. Enhanced chemiluminescence signals on Western blot were analyzed by Gelpro32 Software (Media Cybernetics, Marlow, UK) for quantitative analysis. For immunoprecipitations, equal amounts of protein extracts were incubated with 1 μg of specific antibodies for 16 hours at 4°C. Protein A/G plus agarose beads (Santa Cruz Biotechnology, Dallas, TX) then were added for a 3-hour incubation at 4°C. Normal rabbit or mouse IgG was used as a negative control. Immunoprecipitated proteins were analyzed by immunoblotting. Antibodies used in this work are described in Table 3.

ChIP

Chromatin association analysis was performed in LX-2 cells by chromatin preparation as previously described,[9] immunoprecipitation with antibodies against Sirt6 (MilliporeSigma, St. Louis, MO), Smad3 (Cell Signaling Technology, Danvers, MA), and H3K9Ac (Cell Signaling Technology), and real-time PCR analysis. ChIP DNA amounts for gene promoters of interest were normalized to the input DNA for the same gene sequence. Primers used in the ChIP PCR reactions are described in Table 2.

Statistical Analysis

All statistical data are expressed as means ± SEM. Statistical analysis was performed using Prism 8 software from GraphPad (La Jolla, CA). Comparisons between 2 groups were performed using a 2-tailed Student t test and comparisons for more than 2 groups were performed using 1-way analysis of variance followed by the Tukey post hoc test.

All authors had access to the study data and reviewed and approved the final manuscript.

References

1. Younossi Z, Anstee QM, Marietti M, Hardy T, Henry L, Eslam M, George J, Bugianesi E. Global burden of NAFLD and NASH: trends, predictions, risk factors and prevention. Nat Rev Gastroenterol Hepatol 2018; 15:11–20.
2. Haas JT, Francque S, Staels B. Pathophysiology and mechanisms of nonalcoholic fatty liver disease. Annu Rev Physiol 2016;78:181–205.
3. Tsuchida T, Friedman SL. Mechanisms of hepatic stellate cell activation. Nat Rev Gastroenterol Hepatol 2017; 14:397–411.
4. Schmierer B, Hill CS. TGFbeta-SMAD signal transduction: molecular specificity and functional flexibility. Nat Rev Mol Cell Biol 2007;8:970–982.
5. Inoue Y, Itoh Y, Abe K, Okamoto T, Daitoku H, Fukamizu A, Onozaki K, Hayashi H. Smad3 is acetylated by p300/CBP to regulate its transactivation activity. Oncogene 2007;26:500–508.
6. Kim HG, Huang M, Xin Y, Zhang Y, Zhang X, Wang G, Liu S, Wan J, Ahmadi AR, Sun Z, Liangpunsakul S, Xiong X, Dong XC. The epigenetic regulator SIRT6 protects the liver from alcohol-induced tissue injury by reducing oxidative stress in mice. J Hepatol 2019; 71:960–969.

7. Masri S, Rigor P, Cervantes M, Ceglia N, Sebastian C, Xiao C, Roqueta-Rivera M, Deng C, Osborne TF, Mostoslavsky R, Baldi P, Sassone-Corsi P. Partitioning circadian transcription by SIRT6 leads to segregated control of cellular metabolism. Cell 2014;158:659–672.
8. Tao R, Xiong X, DePinho RA, Deng CX, Dong XC. FoxO3 transcription factor and Sirt6 deacetylase regulate low density lipoprotein (LDL)-cholesterol homeostasis via control of the proprotein convertase subtilisin/kexin type 9 (Pcsk9) gene expression. J Biol Chem 2013; 288:29252–29259.
9. Tao R, Xiong X, DePinho RA, Deng CX, Dong XC. Hepatic SREBP-2 and cholesterol biosynthesis are regulated by FoxO3 and Sirt6. J Lipid Res 2013; 54:2745–2753.
10. Elhanati S, Kanfi Y, Varvak A, Roichman A. Carmel-Gross I, Barth S, Gibor G, Cohen HY. Multiple regulatory layers of SREBP1/2 by SIRT6. Cell Rep 2013; 4:905–912.
11. Sebastian C, Zwaans BM, Silberman DM, Gymrek M, Goren A, Zhong L, Ram O, Truelove J, Guimaraes AR, Toiber D, Cosentino C, Greenson JK, MacDonald AI, McGlynn L, Maxwell F, Edwards J, Giacosa S, Guccione E, Weissleder R, Bernstein BE, Regev A, Shiels PG, Lombard DB, Mostoslavsky R. The histone deacetylase SIRT6 is a tumor suppressor that controls cancer metabolism. Cell 2012;151:1185–1199.
12. Dominy JE Jr, Lee Y, Jedrychowski MP, Chim H, Jurczak MJ, Camporez JP, Ruan HB, Feldman J, Pierce K, Mostoslavsky R, Denu JM, Clish CB, Yang X, Shulman GI, Gygi SP, Puigserver P. The deacetylase Sirt6 activates the acetyltransferase GCN5 and suppresses hepatic gluconeogenesis. Mol Cell 2012; 48:900–913.
13. Zhong L, D'Urso A, Toiber D, Sebastian C, Henry RE, Vadysirisack DD, Guimaraes A, Marinelli B, Wikstrom JD, Nir T, Clish CB, Vaitheesvaran B, Iliopoulos O, Kurland I, Dor Y, Weissleder R, Shirihai OS, Ellisen LW, Espinosa JM, Mostoslavsky R. The histone deacetylase Sirt6 regulates glucose homeostasis via Hif1alpha. Cell 2010;140:280–293.
14. Kim HS, Xiao C, Wang RH, Lahusen T, Xu X, Vassilopoulos A, Vazquez-Ortiz G, Jeong WI, Park O, Ki SH, Gao B, Deng CX. Hepatic-specific disruption of SIRT6 in mice results in fatty liver formation due to enhanced glycolysis and triglyceride synthesis. Cell Metab 2010;12:224–236.
15. Kanfi Y, Peshti V, Gil R, Naiman S, Nahum L, Levin E, Kronfeld-Schor N, Cohen HY. SIRT6 protects against pathological damage caused by diet-induced obesity. Aging Cell 2010;9:162–173.
16. Mostoslavsky R, Chua KF, Lombard DB, Pang WW, Fischer MR, Gellon L, Liu P, Mostoslavsky G, Franco S, Murphy MM, Mills KD, Patel P, Hsu JT, Hong AL, Ford E, Cheng HL, Kennedy C, Nunez N, Bronson R, Frendewey D, Auerbach W, Valenzuela D, Karow M, Hottiger MO, Hursting S, Barrett JC, Guarente L, Mulligan R, Demple B, Yancopoulos GD, Alt FW. Genomic instability and aging-like phenotype in the absence of mammalian SIRT6. Cell 2006;124:315–329.
17. Jiang H, Khan S, Wang Y, Charron G, He B, Sebastian C, Du J, Kim R, Ge E, Mostoslavsky R, Hang HC, Hao Q, Lin H. SIRT6 regulates TNF-alpha secretion through hydrolysis of long-chain fatty acyl lysine. Nature 2013; 496:110–113.
18. Pan PW, Feldman JL, Devries MK, Dong A, Edwards AM, Denu JM. Structure and biochemical functions of SIRT6. J Biol Chem 2011;286:14575–14587.
19. Michishita E, McCord RA, Berber E, Kioi M, Padilla-Nash H, Damian M, Cheung P, Kusumoto R, Kawahara TL, Barrett JC, Chang HY, Bohr VA, Ried T, Gozani O, Chua KF. SIRT6 is a histone H3 lysine 9 deacetylase that modulates telomeric chromatin. Nature 2008;452:492–496.
20. Ka SO, Bang IH, Bae EJ, Park BH. Hepatocyte-specific sirtuin 6 deletion predisposes to nonalcoholic steatohepatitis by up-regulation of Bach1, an Nrf2 repressor. FASEB J 2017;31:3999–4010.
21. Xiao C, Wang RH, Lahusen TJ, Park O, Bertola A, Maruyama T, Reynolds D, Chen Q, Xu X, Young HA, Chen WJ, Gao B, Deng CX. Progression of chronic liver inflammation and fibrosis driven by activation of c-JUN signaling in Sirt6 mutant mice. J Biol Chem 2012; 287:41903–41913.
22. Luo P, Qin C, Zhu L, Fang C, Zhang Y, Zhang H, Pei F, Tian S, Zhu XY, Gong J, Mao Q, Xiao C, Su Y, Zheng H, Xu T, Lu J, Zhang J. Ubiquitin-specific peptidase 10 (USP10) inhibits hepatic steatosis, insulin resistance, and inflammation through Sirt6. Hepatology 2018;68:1786–1803.
23. Maity S, Muhamed J, Sarikhani M, Kumar S, Ahamed F, Spurthi KM, Ravi V, Jain A, Khan D, Arathi BP, Desingu PA, Sundaresan NR. Sirtuin 6 deficiency transcriptionally up-regulates TGF-beta signaling and induces fibrosis in mice. J Biol Chem 2020;295:415–434.
24. Tian K, Chen P, Liu Z, Si S, Zhang Q, Mou Y, Han L, Wang Q, Zhou X. Sirtuin 6 inhibits epithelial to mesenchymal transition during idiopathic pulmonary fibrosis via inactivating TGF-beta1/Smad3 signaling. Oncotarget 2017;8:61011–61024.
25. Zhang Q, Tu W, Tian K, Han L, Wang Q, Chen P, Zhou X. Sirtuin 6 inhibits myofibroblast differentiation via inactivating transforming growth factor-beta1/Smad2 and nuclear factor-kappaB signaling pathways in human fetal lung fibroblasts. J Cell Biochem 2019;120:93–104.
26. Newberry EP, Xie Y, Lodeiro C, Solis R, Moritz W, Kennedy S, Barron L, Onufer E, Alpini G, Zhou T, Blaner WS, Chen A, Davidson NO. Hepatocyte and stellate cell deletion of liver fatty acid binding protein reveals distinct roles in fibrogenic injury. FASEB J 2019; 33:4610–4625.
27. Lee Y, Ka SO, Cha HN, Chae YN, Kim MK, Park SY, Bae EJ, Park BH. Myeloid sirtuin 6 deficiency causes insulin resistance in high-fat diet-fed mice by eliciting macrophage polarization toward an M1 phenotype. Diabetes 2017;66:2659–2668.
28. Xiong X, Wang G, Tao R, Wu P, Kono T, Li K, Ding WX, Tong X, Tersey SA, Harris RA, Mirmira RG, Evans-Molina C, Dong XC. Sirtuin 6 regulates glucose-stimulated insulin secretion in mouse pancreatic beta cells. Diabetologia 2016;59:151–160.

29. Van Meter M, Simon M, Tombline G, May A, Morello TD, Hubbard BP, Bredbenner K, Park R, Sinclair DA, Bohr VA, Gorbunova V, Seluanov A. JNK Phosphorylates SIRT6 to stimulate DNA double-strand break repair in response to oxidative stress by recruiting PARP1 to DNA breaks. Cell Rep 2016;16:2641–2650.
30. Kugel S, Sebastian C, Fitamant J, Ross KN, Saha SK, Jain E, Gladden A, Arora KS, Kato Y, Rivera MN, Ramaswamy S, Sadreyev RI, Goren A, Deshpande V, Bardeesy N, Mostoslavsky R. SIRT6 suppresses pancreatic cancer through control of Lin28b. Cell 2016; 165:1401–1415.
31. Elhanati S, Ben-Hamo R, Kanfi Y, Varvak A, Glazz R, Lerrer B, Efroni S, Cohen HY. Reciprocal regulation between SIRT6 and miR-122 controls liver metabolism and predicts hepatocarcinoma prognosis. Cell Rep 2016; 14:234–242.
32. Zhang P, Tu B, Wang H, Cao Z, Tang M, Zhang C, Gu B, Li Z, Wang L, Yang Y, Zhao Y, Wang H, Luo J, Deng CX, Gao B, Roeder RG, Zhu WG. Tumor suppressor p53 cooperates with SIRT6 to regulate gluconeogenesis by promoting FoxO1 nuclear exclusion. Proc Natl Acad Sci U S A 2014;111:10684–10689.
33. Xiong X, Tao R, DePinho RA, Dong XC. Deletion of hepatic FoxO1/3/4 genes in mice significantly impacts on glucose metabolism through downregulation of gluconeogenesis and upregulation of glycolysis. PLoS One 2013;8:e74340.
34. Toiber D, Erdel F, Bouazoune K, Silberman DM, Zhong L, Mulligan P, Sebastian C, Cosentino C, Martinez-Pastor B, Giacosa S, D'Urso A, Naar AM, Kingston R, Rippe K, Mostoslavsky R. SIRT6 recruits SNF2H to DNA break sites, preventing genomic instability through chromatin remodeling. Mol Cell 2013;51:454–468.
35. Marquardt JU, Fischer K, Baus K, Kashyap A, Ma S, Krupp M, Linke M, Teufel A, Zechner U, Strand D, Thorgeirsson SS, Galle PR, Strand S. Sirtuin-6-dependent genetic and epigenetic alterations are associated with poor clinical outcome in hepatocellular carcinoma patients. Hepatology 2013;58:1054–1064.
36. Min L, Ji Y, Bakiri L, Qiu Z, Cen J, Chen X, Chen L, Scheuch H, Zheng H, Qin L, Zatloukal K, Hui L, Wagner EF. Liver cancer initiation is controlled by AP-1 through SIRT6-dependent inhibition of survivin. Nat Cell Biol 2012;14:1203–1211.
37. Mao Z, Tian X, Van Meter M, Ke Z, Gorbunova V, Seluanov A. Sirtuin 6 (SIRT6) rescues the decline of homologous recombination repair during replicative senescence. Proc Natl Acad Sci U S A 2012; 109:11800–11805.
38. Kanfi Y, Naiman S, Amir G, Peshti V, Zinman G, Nahum L, Bar-Joseph Z, Cohen HY. The sirtuin SIRT6 regulates lifespan in male mice. Nature 2012; 483:218–221.
39. Mao Z, Hine C, Tian X, Van Meter M, Au M, Vaidya A, Seluanov A, Gorbunova V. SIRT6 promotes DNA repair under stress by activating PARP1. Science 2011; 332:1443–1446.
40. Kaidi A, Weinert BT, Choudhary C, Jackson SP. Human SIRT6 promotes DNA end resection through CtIP deacetylation. Science 2010;329:1348–1353.
41. Yang B, Zwaans BM, Eckersdorff M, Lombard DB. The sirtuin SIRT6 deacetylates H3 K56Ac in vivo to promote genomic stability. Cell Cycle 2009;8:2662–2663.
42. Van Gool F, Galli M, Gueydan C, Kruys V, Prevot PP, Bedalov A, Mostoslavsky R, Alt FW, De Smedt T, Leo O. Intracellular NAD levels regulate tumor necrosis factor protein synthesis in a sirtuin-dependent manner. Nat Med 2009;15:206–210.
43. Kawahara TL, Michishita E, Adler AS, Damian M, Berber E, Lin M, McCord RA, Ongaigui KC, Boxer LD, Chang HY, Chua KF. SIRT6 links histone H3 lysine 9 deacetylation to NF-kappaB-dependent gene expression and organismal life span. Cell 2009;136:62–74.
44. Xiong X, Sun X, Wang Q, Qian X, Zhang Y, Pan X, Dong XC. SIRT6 protects against palmitate-induced pancreatic beta-cell dysfunction and apoptosis. J Endocrinol 2016;231:159–165.
45. Oussaief L, Hippocrate A, Ramirez V, Rampanou A, Zhang W, Meyers D, Cole P, Khelifa R, Joab I. Phosphatidylinositol 3-kinase/Akt pathway targets acetylation of Smad3 through Smad3/CREB-binding protein interaction: contribution to transforming growth factor beta1-induced Epstein-Barr virus reactivation. J Biol Chem 2009;284:23912–23924.
46. Postic C, Shiota M, Niswender KD, Jetton TL, Chen Y, Moates JM, Shelton KD, Lindner J, Cherrington AD, Magnuson MA. Dual roles for glucokinase in glucose homeostasis as determined by liver and pancreatic beta cell-specific gene knock-outs using Cre recombinase. J Biol Chem 1999;274:305–315.
47. Kuhn R, Schwenk F, Aguet M, Rajewsky K. Inducible gene targeting in mice. Science 1995;269:1427–1429.
48. Mederacke I, Hsu CC, Troeger JS, Huebener P, Mu X, Dapito DH, Pradere JP, Schwabe RF. Fate tracing reveals hepatic stellate cells as dominant contributors to liver fibrosis independent of its aetiology. Nat Commun 2013;4:2823.
49. Schwenk F, Baron U, Rajewsky K. A cre-transgenic mouse strain for the ubiquitous deletion of loxP-flanked gene segments including deletion in germ cells. Nucleic Acids Res 1995;23:5080–5081.
50. Kwon HJ, Won YS, Park O, Chang B, Duryee MJ, Thiele GE, Matsumoto A, Singh S, Abdelmegeed MA, Song BJ, Kawamoto T, Vasiliou V, Thiele GM, Gao B. Aldehyde dehydrogenase 2 deficiency ameliorates alcoholic fatty liver but worsens liver inflammation and fibrosis in mice. Hepatology 2014;60:146–157.
51. Tao R, Wei D, Gao H, Liu Y, DePinho RA, Dong XC. Hepatic FoxOs regulate lipid metabolism via modulation of expression of the nicotinamide phosphoribosyltransferase gene. J Biol Chem 2011;286:14681–14690.
52. Huang M, Kim HG, Zhong X, Dong C, Zhang B, Fang Z, Zhang Y, Lu X, Saxena R, Liu Y, Zhang C, Liangpunsakul S, Dong XC. Sestrin 3 protects against diet-induced nonalcoholic steatohepatitis in mice through suppression of transforming growth factor beta signal transduction. Hepatology 2020;71:76–92.

Received January 12, 2020. Accepted April 9, 2020.

Correspondence
Address correspondence to: X. Charlie Dong, PhD, Department of Biochemistry and Molecular Biology, Indiana University School of Medicine, 635 Barnhill Drive, MS-1021D, Indianapolis, Indiana 46202. e-mail: xcdong@iu.edu; fax: (317) 274-4686.

Author contributions
Xiaolin Zhong, Menghao Huang, and Hyeong-Geug Kim were responsible for the acquisition of data, analysis and interpretation of data, and drafting of the manuscript; Yang Zhang, Kushan Chowdhury, and Wenjie Cai were responsible for the acquisition of data; Romil Saxena and Robert F. Schwabe provided material support; Suthat Liangpunsakul critically revised the manuscript and provided material support; and X. Charlie Dong was responsible for the study concept and design, analysis and interpretation of data, drafting of the manuscript, statistical analysis, obtaining funding, and study supervision.

Conflicts of interest
The authors disclose no conflicts.

Funding
This study was supported in part by National Institutes of Health grants R56DK091592 (X.C.D.), R21AA024550 (X.C.D.), and R01DK107682 (S.L. and X.C.D.); Wang Bao En Liver Fibrosis Foundation grant CFHPC 2020052 (X.Z.); Luzhou Science and Technology Bureau project 2019LZXNYDJ27 (X.Z.); Science and Technology Department of Sichuan Province grant 20YYJC1989 (X.Z.); Indiana Diabetes Research Center National Institutes of Health grant P30DK097512; and Indiana Clinical and Translational Sciences Institute funded by the National Institutes of Health National Center for Advancing Translational Sciences clinical and translational science award UL1TR002529. The sponsors had no role in the study design and data collection, analysis, or interpretation.